Electronic Supplementary Information

Ring-opening polymerization of *rac*-lactide mediated by tetrametallic lithium and sodium diamino-bis(phenolate) complexes

Dalal Alhashmialameer,[a] Nduka Ikpo,[a] Julie Collins,[b] Louise N. Dawe,[abc] Karen Hattenhauer,[a] and Francesca M. Kerton*[a]

[a] Department of Chemistry, Memorial University of Newfoundland, St. John's, Newfoundland, Canada A1B 3X7. E-mail: fkerton@mun.ca

[b] C-CART X-ray Diffraction Laboratory, Memorial University of Newfoundland, St. John's, Newfoundland.

[C] Current Address: Department of Chemistry, Wilfrid Laurier University, Waterloo, Ontario, Canada.

Table S1. Crystallographic data and structure refinement for **1** and **4**. S3
Table S2. Selected Bond lengths (Å) and angles (°) for **1** and **4**. S4
Figure S1. ^{1}H NMR spectrum (300 MHz, 298 K, C_6D_6) of **1**. S5
Figure S2. ^{1}H NMR spectrum (500 MHz, 298 K, C_6D_6 and C_5D_5N) of **1**. S6
Figure S3. ^{1}H NMR spectrum (500 MHz, 298 K, C_5D_5N) of **1**. S7
Figure S4. ^{7}Li NMR spectrum (300 MHz, 298 K, C_6D_6) of **4**. S8
Figure S5. ^{1}H NMR spectrum (300 MHz, 298 K, C_6D_6) of **4**. S9
Figure S6a. ^{1}H NMR spectrum (500 MHz, 233 K, C_5D_5N) of **4**. S10
Figure S6b. ^{1}H NMR spectrum (500 MHz, 308 K, C_5D_5N) of **4**. S11
Figure S7. Conversion (%) vs. time for the ROP of LA initiated by **3** under the conditions in Table 1, entry 9. S12
Figure S8. Conversion (%) vs. time for the ROP of LA initiated by **3** under the conditions in Table 2, entries 13, 15 and 17. CH_2Cl_2, Toluene, THF. S12
Figure S9. First-order plot of LA consumption initiated by **3** according to the conditions in Table 2, entries 13 and 15. CH_2Cl_2 ($y = 0.0256x + 0.1897$, $R^2 = 0.9894$), Toluene ($y = 0.0884x + 0.3487$, $R^2 = 0.9593$). S13
Figure S10. Conversion (%) vs. time for the ROP of LA initiated by **1**, **2**, **3** and **4** in CH_2Cl_2 under the conditions in Table 2, entries 2, 8, 13 and 19. **1**, **2**, **3**, **4**. S13
Figure S11. First-order plot of LA consumption initiated by **1**, **2**, **3** and **4** in CH_2Cl_2 under conditions in Table 2, entries 2, and 13. **1** ($y = 0.0114x + 0.0834$, $R^2 = 0.96$), **3** ($y = 0.0257x + 0.2068$, $R^2 = 0.9983$). S14
Figure S12. Conversion (%) vs. time for the ROP of LA initiated by **1** in CH_2Cl_2 under the conditions in Table 2, entries 2, 3 and 5. **1 eq. BnOH**, **2 eq. BnOH**, **4 eq. BnOH**. S14
Figure S13. ^{1}H NMR spectrum in $CDCl_3$ of PLA obtained under the conditions in Table 2, entry 12, similar spectra also obtained for entries 13, 18 and 19. S15

Figure S14. ^{1}H NMR spectrum in $CDCl_3$ of PLA obtained under the conditions in Table 2, entry 3, similar spectrum obtained for entry 5. S16
Figure S15. $^{1}H\{^{1}H\}$NMR spectrum (500 MHz, $CDCl_3$) of the methine region of PLA produced under the conditions in Table 2, entry 7, similar results were obtained for entries 8, 12 and 13. S17
Figure S16. ^{13}C NMR spectrum (500 MHz, $CDCl_3$) of the methine region of PLA produced under the conditions in Table 2, entry 7, similar results were obtained for entries 8, 12 and 13. S17
Figure S17. ^{7}Li NMR spectrum (300 MHz, C_6D_6) of **1** with and without 1 equiv. *rac*-lactide. S18
Figure S18. Monitoring of stoichiometric (M: BnOH: LA, 1:1 and 1:1:1) model reactions by ^{1}H NMR in dichloromethane-d_2 at 298 K (500 MHz). S19
Figure S19. Monitoring of stoichiometric (M: BnOH: LA, 1:2 and 1:2:1) model reactions by ^{1}H NMR in dichloromethane-d_2 at 298 K (500 MHz). S20
Figure S20. Monitoring of stoichiometric (M: BnOH: LA, 1:4 and 1:4:1) model reactions by ^{1}H NMR in dichloromethane-d_2 at 298 K (500 MHz). S21
Figure S21. ^{13}C NMR spectrum (300 MHz, 298 K, $CDCl_3$) of **1**. S22
Figure S22. ^{13}C NMR spectrum (300 MHz, 298 K, C_6D_6) of **1**. S23
Figure S23. ^{13}C NMR spectrum (300 MHz, 298 K, C_5D_5N) of **1**. S24
Figure S24. MALDI-TOF spectrum of **1**. S25
Figure S25. Theoretical and Experimental MALDI-TOF MS isotopic distribution pattern for **1**. S25
Figure S26. ^{1}H NMR spectrum (300 MHz, 298 K, C_6D_6) of **2**. S26
Figure S27. ^{13}C NMR spectrum (300 MHz, 298 K, C_5D_5N) of **2**. S27
Figure S28. ^{13}C NMR spectrum (300 MHz, 298 K, $CDCl_3$) of **2**. S28
Figure S29. MALDI-TOF spectrum of **2**. S29
Figure S30. Theoretical and Experimental MALDI-TOF MS isotopic distribution pattern for **2**. S29
Figure S31. ^{1}H NMR spectrum (300 MHz, 298 K, C_6D_6) of **3**. S30
Figure S32. ^{13}C NMR spectrum (300 MHz, 298 K, C_6D_6) of **3**. S31
Figure S33. MALDI-TOF spectrum of **3**. S32
Figure S34. Theoretical and Experimental MALDI-TOF MS isotopic distribution pattern for **3**. S32
Figure S35. ^{13}C NMR spectrum (300 MHz, 298 K, $CDCl_3$) of **4**. S33
Figure S36. MALDI-TOF spectrum of **4**. S34

Table S1. Crystallographic data and structure refinement for **1** and **4**.

Compound	**1** (CCDC 1410026)	**4** (CCDC 1410027)
Empirical Formula	$C_{82}H_{132}Li_4N_4O_7$ .3(C_7H_8)	$C_{66}H_{100}Na_4N_4O_6$
Formula Weight	1590.15	1137.51
Temperature/K	163	163
Crystal Color	Colorless	Colorless
Crystal System	Triclinic	Monoclinic
Crystal Dimensions	0.38 X 0.35 X 0.34 mm	0.5 × 0.43 × 0.35 mm
Lattice Parameters	a = 16.592(2) Å	a = 12.898(4) Å
	b = 18.655(2) Å	b = 13.741(4) Å
	c = 19.067(2) Å	c = 18.695(6) Å
	α = 103.219(7)°	α = 90°
	β = 98.581(7)°	β = 101.518(4)°
	V = 5265.8(10) $Å^3$	V = 3246.7(17) Å
Space Group	P-1 (#2)	$P2_1/n$
Z value	2	2
D_{calc}	1.003 g/cm^3	1.164 g/cm^3
F_{000}	1740	1232.0
μ(MoKα)	0.61 cm^{-1}	0.096 cm^{-1}
Reflections collected	43063	24304
Independent reflections	21429	7155
R_{int}	0.0454	0.0374
R, wR_2 (all)[a]	0.1462, 0.3597	0.0604, 0.1653
R, wR_2 [I>=2σ (I)][a]	0.1130, 0.3441	0.0543, 0.1580
GOF-fit on F^2	1.060	1.084

[a] $R_1 = \Sigma(|F_o| - |F_c|)/\Sigma|F_o|$; $wR_2 = [\ \Sigma(w(F_o^2 - F_c^2)^2)/\ \Sigma w(F_o^2)^2\ ]^{1/2}$

Table S2. Selected Bond lengths (Å) and angles (°) for **1** and **4**.

1		**4**	
Li(1)-O(1)	1.804(8)	Na(1)-O(1)	2.3450(14)
Li(2)-O(1)	1.932(7)	Na(1)-O(2)	2.3176(14)
Li(1)-O(3)	1.849(8)	Na(1)-O(4)	2.3956(13)
Li(2)-O(3)	1.924(7)	Na(1)-N(2)	2.6392(16)
Li(1)-O(5)	1.932(8)	Na(2)-O(4)	2.1825(14)
Li(2)-N(1)	2.268(8)	Na(2)-O(2)	2.2369(17)
Li(2)-N(3)	2.295(7)	Na(1)-N(1)	2.6761(16)
O(1)-Li(1)-O(3)	100.0(4)	O(1)-Na(1)-O(4)	89.16(4)
O1-Li(1)-O(3)	130.5(4)	O(1)-Na(1)-N(2)	134.44(5)
O(1)-Li(2)-O(3)	93.0(3)	O(4)-Na(1)-N(2)	123.34(5)
Li(1)-O(1)-Li(2)	50.3(2)	O(1)-Na(1)-N(1)	77.30(4)
Li(1)-O(3)-Li(2)	50.0(2)	O(2)-Na(1)-O(4)	92.48(5)
O(1)-Li(2)-N(1)	95.5(3)	O(2)-Na(1)-N(2)	77.34(5)
O(1)-Li(2)-N(3)	123.4(3)	O(2)-Na(1)-N(1)	139.96(5)
O(3)-Li(2)-N(1)	118.7(3)	N(1)-Na(1)-N(2)	62.65(5)
O(3)-Li(2)-N(3)	94.3(3)	O(2)-Na(1)-O(4)	35.63(4)
N(1)-Li(2)-N(3)	128.0(3)		

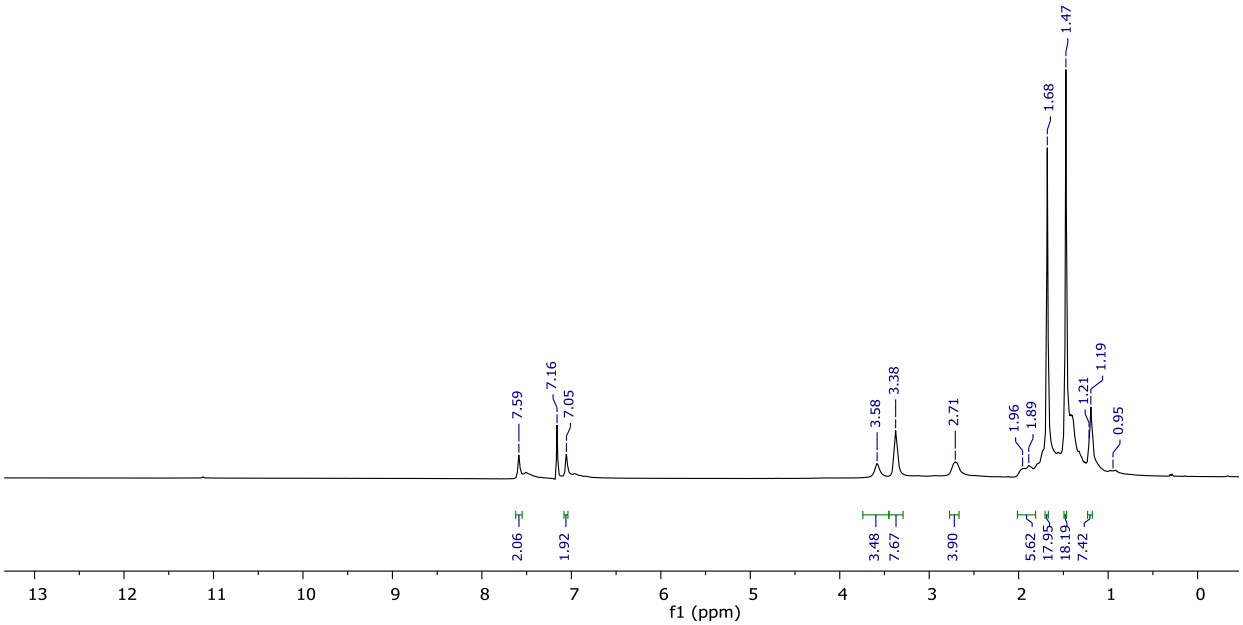

Figure S1. ^{1}H NMR spectrum (300 MHz, 298 K, C_6D_6) of **1**.

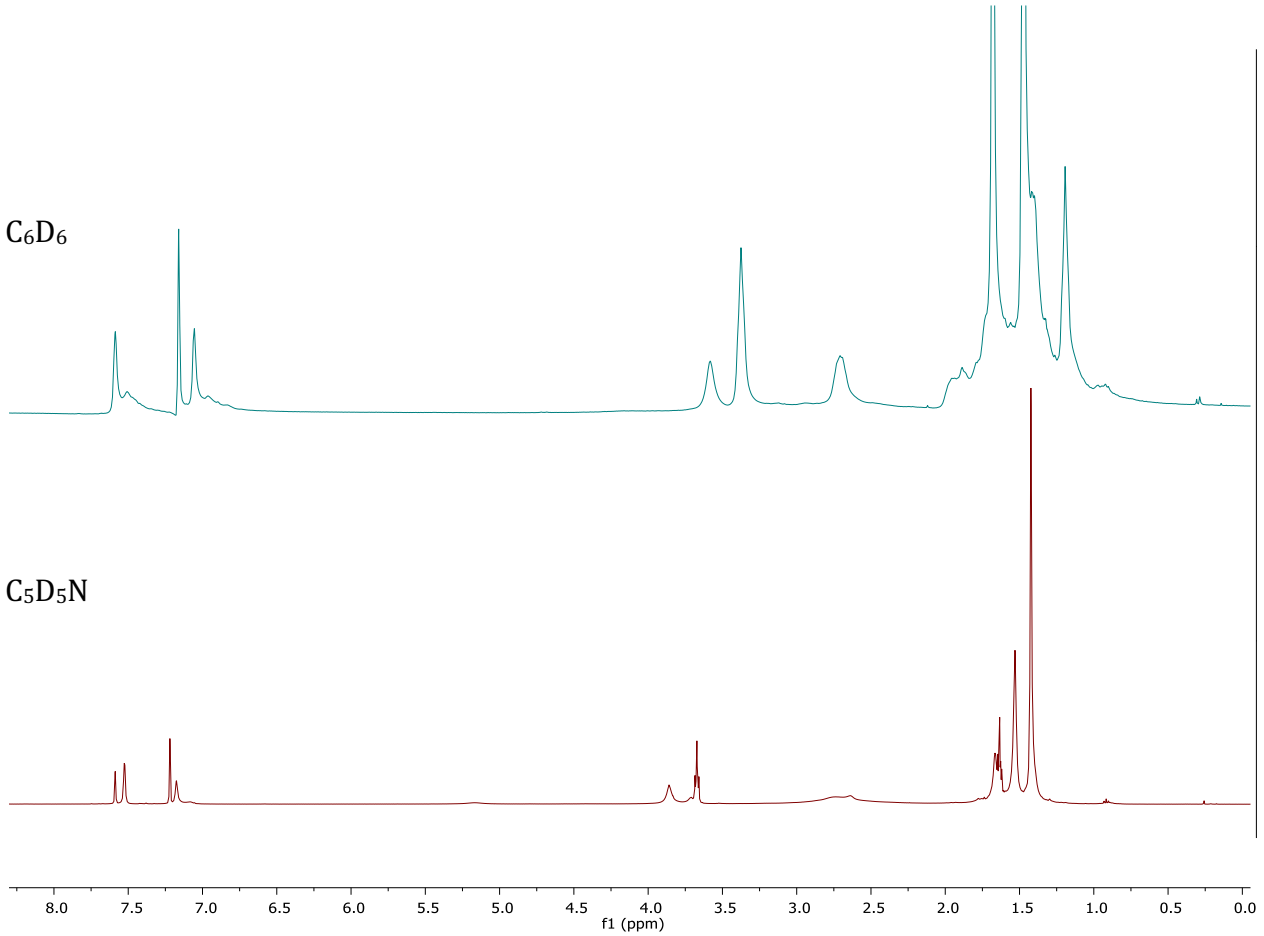

Figure S2. ^{1}H NMR spectrum (500 MHz, 298 K, C_6D_6 and C_5D_5N) of **1**.

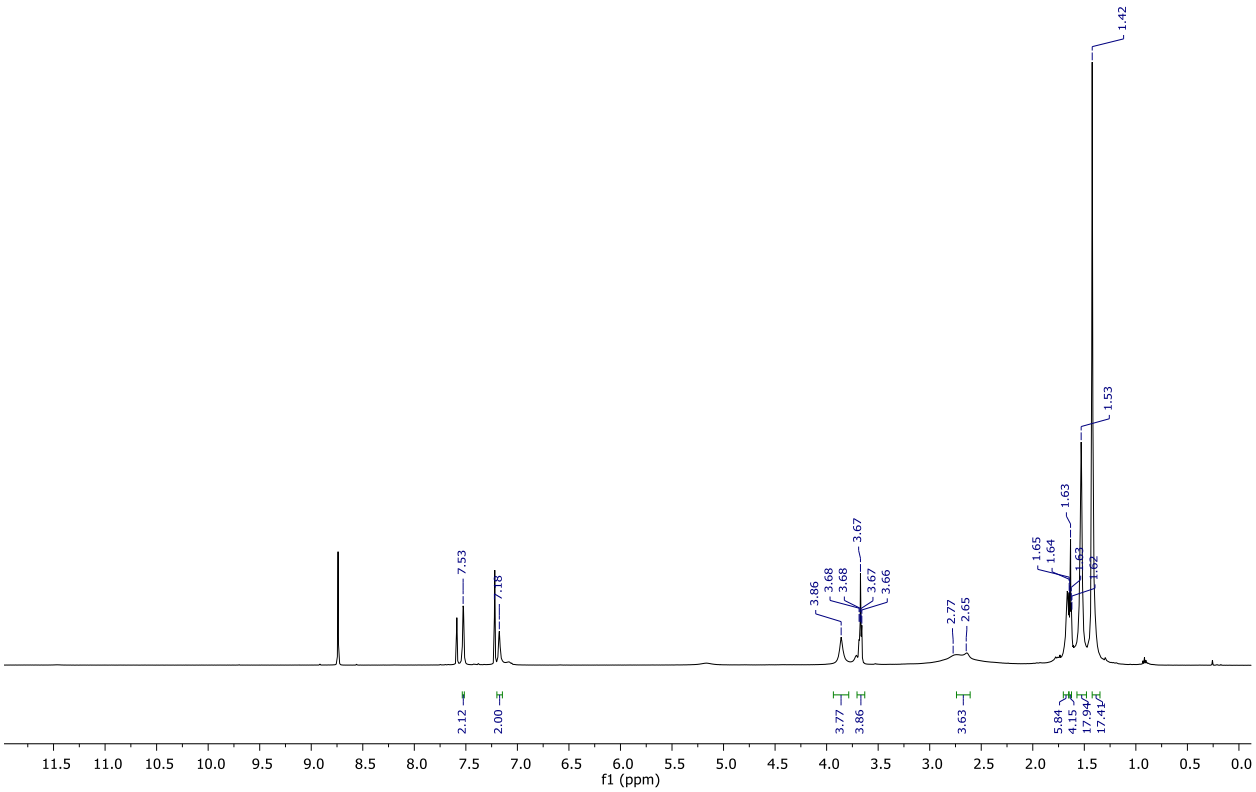

Figure S3. ^{1}H NMR spectrum (500 MHz, 298 K, C_5D_5N) of **1**.

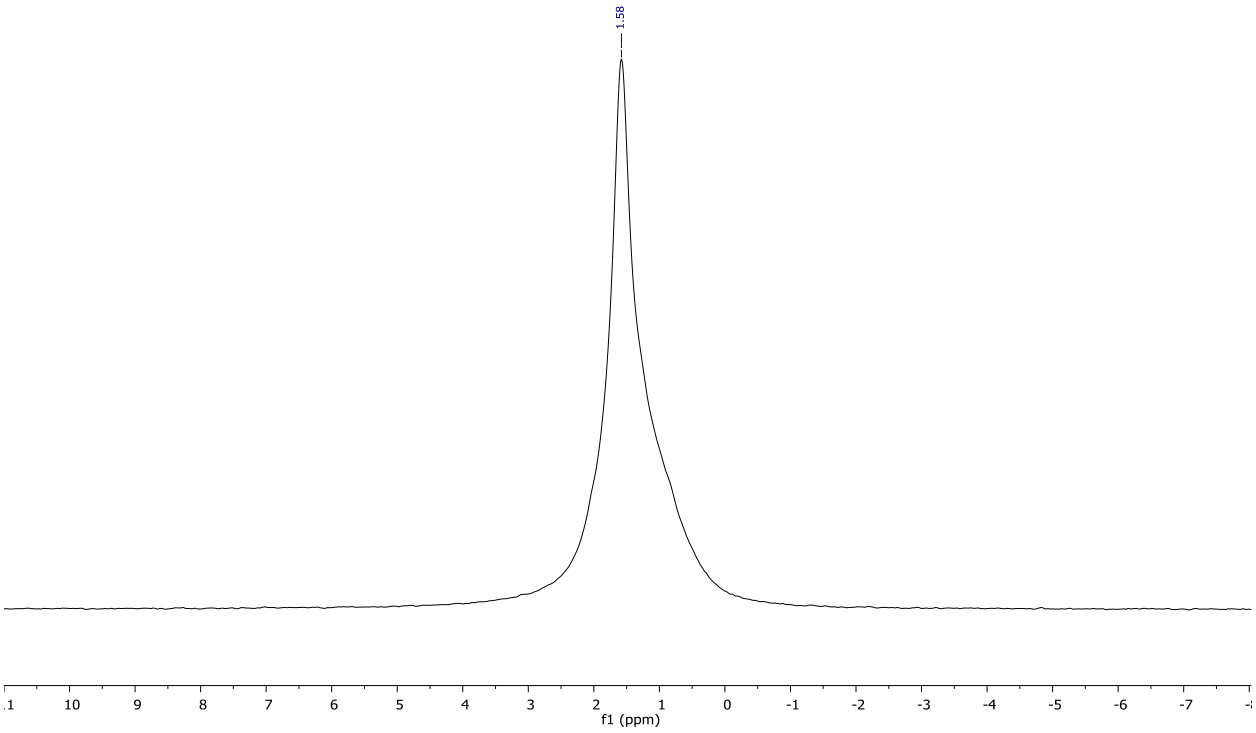

Figure S4. ^{7}Li NMR spectrum (300 MHz, 298 K, C_6D_6) of **1**.

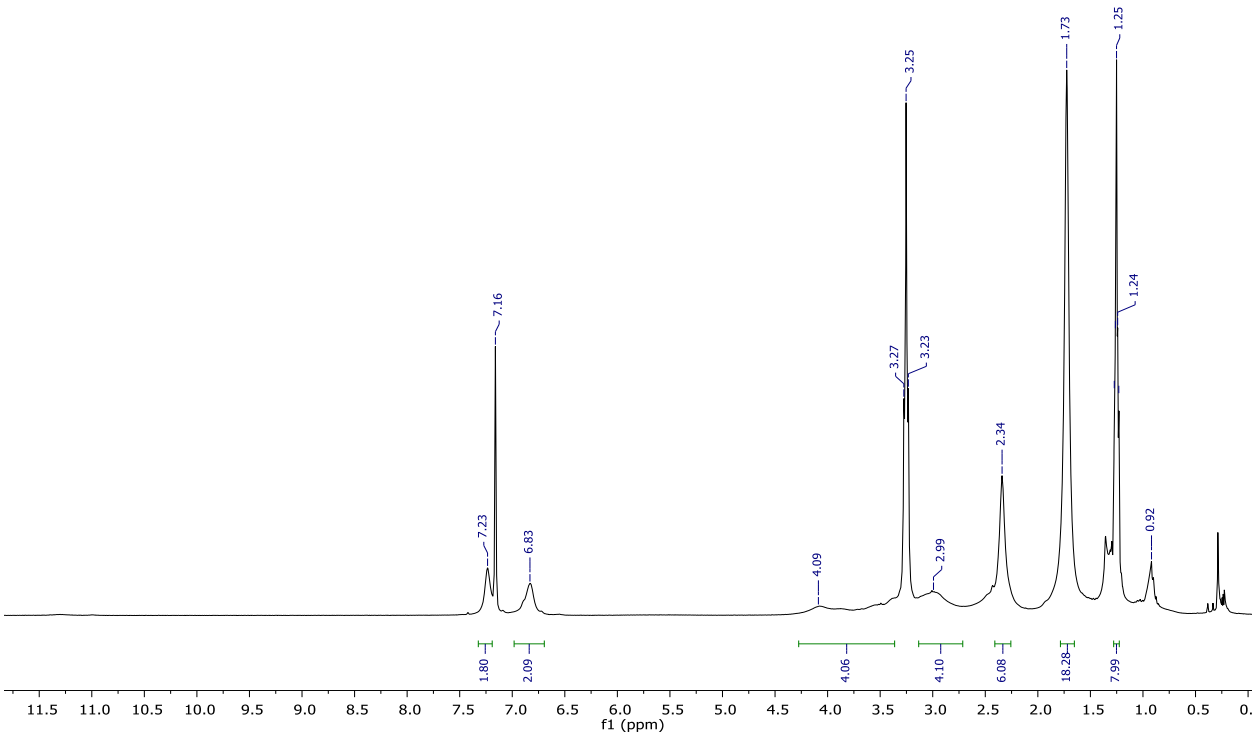

Figure S5. ^{1}H NMR spectrum (300 MHz, 298 K, C_6D_6) of **4**.

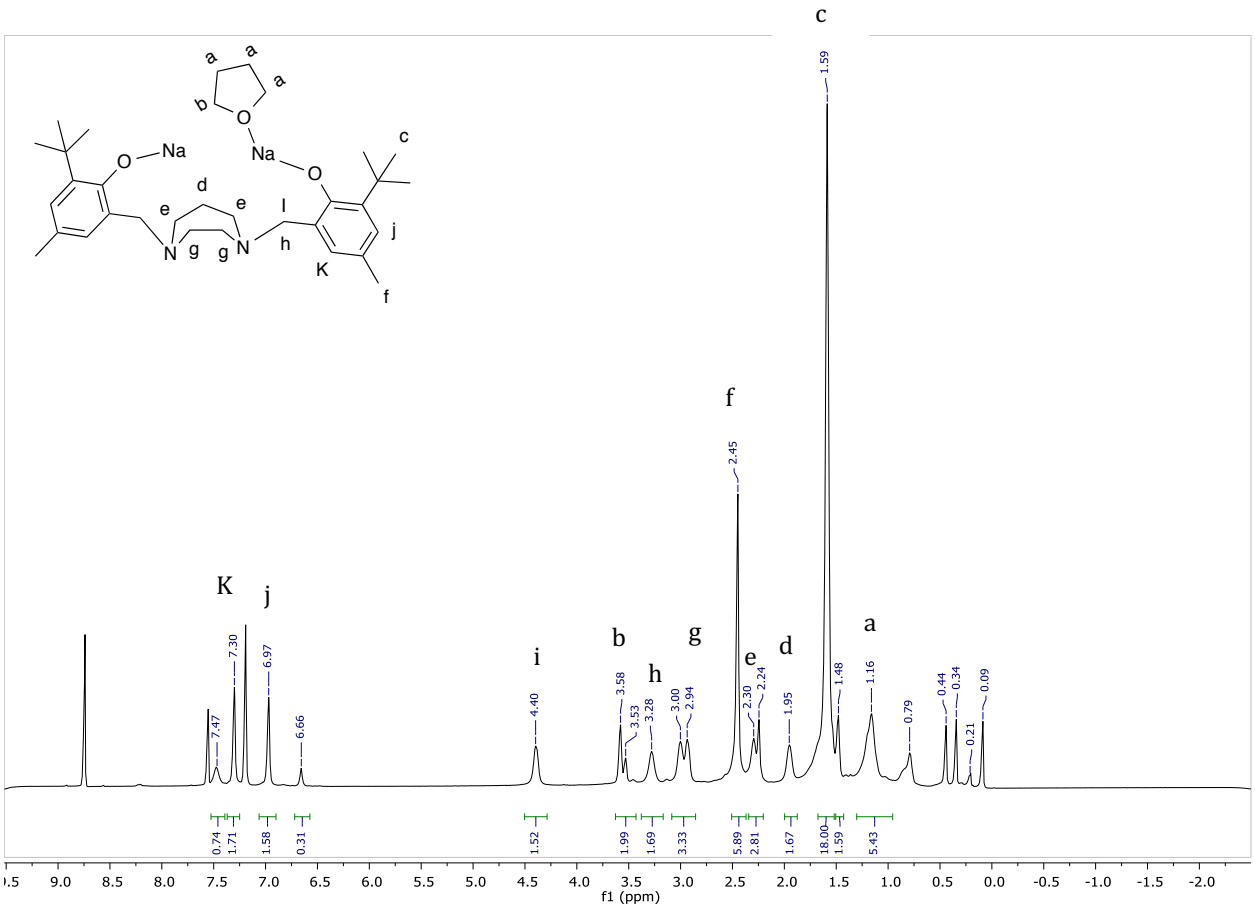

Figure S6a. ^{1}H NMR spectrum (500 MHz, 233 K, C_5D_5N) of **4**.

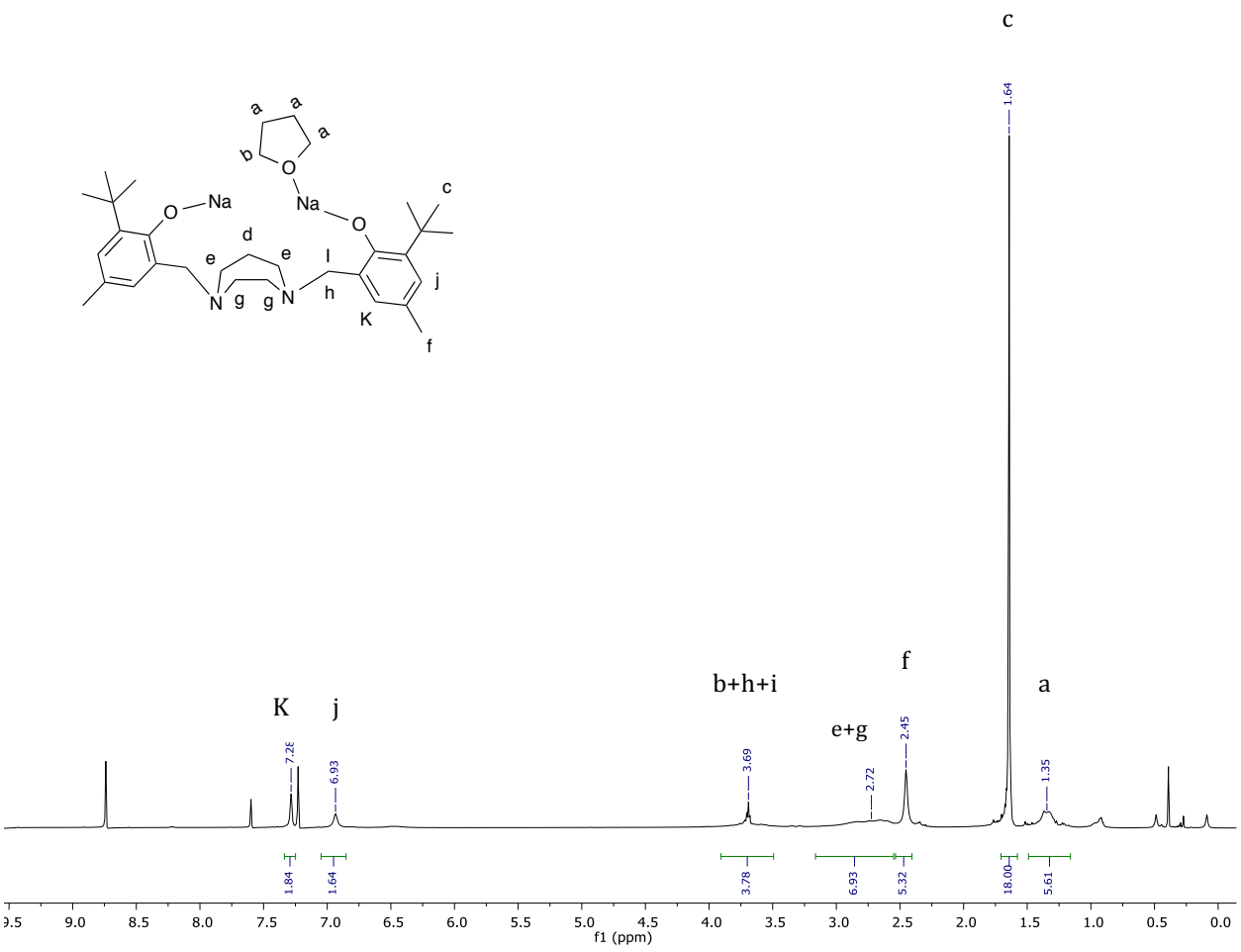

Figure S6b. ^{1}H NMR spectrum (500 MHz, 308 K, C_5D_5N) of **4**.

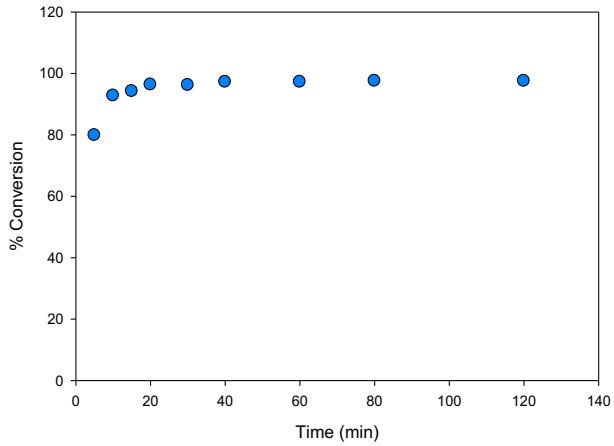

Figure S7. Conversion (%) vs. time for the ROP of LA initiated by **3** under the conditions in Table 1, entry 9.

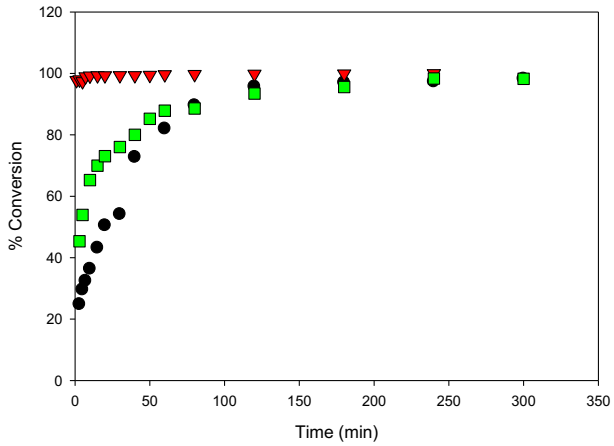

Figure S8. Conversion (%) vs. time for the ROP of LA initiated by **3** under the conditions in Table 2, entries 13, 15 and 17. CH_2Cl_2, Toluene, THF.

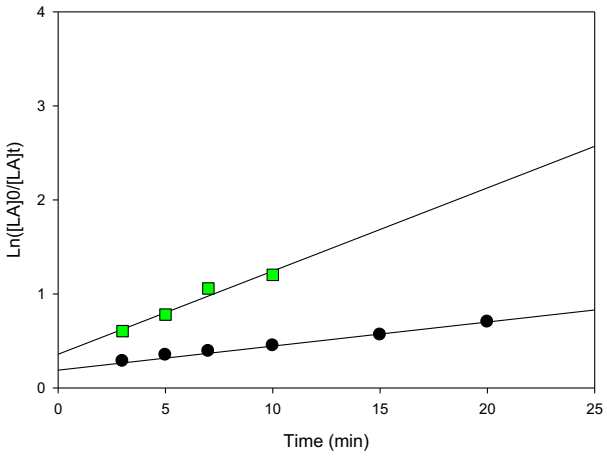

Figure S9. First-order plot of LA consumption initiated by **3** according to the conditions in Table 2, entries 13 and 15. CH_2Cl_2 (y = 0.0256x + 0.1897, R^2 = 0.9894), Toluene (y = 0.0884x + 0.3487, R^2 = 0.9593).

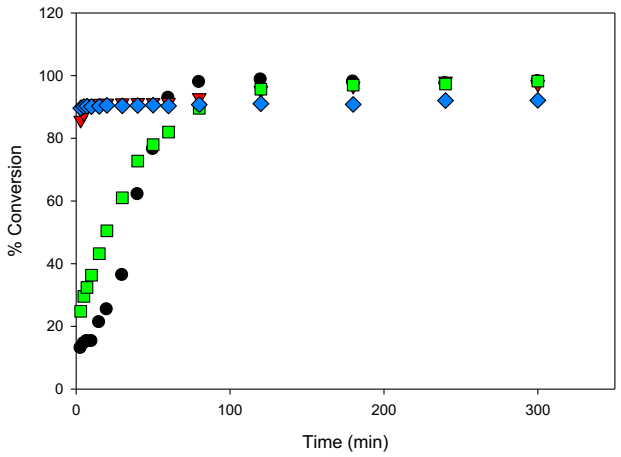

Figure S10. Conversion (%) vs. time for the ROP of LA initiated by **1**, **2**, **3** and **4** in CH_2Cl_2 under the conditions in Table 2, entries 2, 8, 13 and 19. **1**, **2**, **3**, **4**.

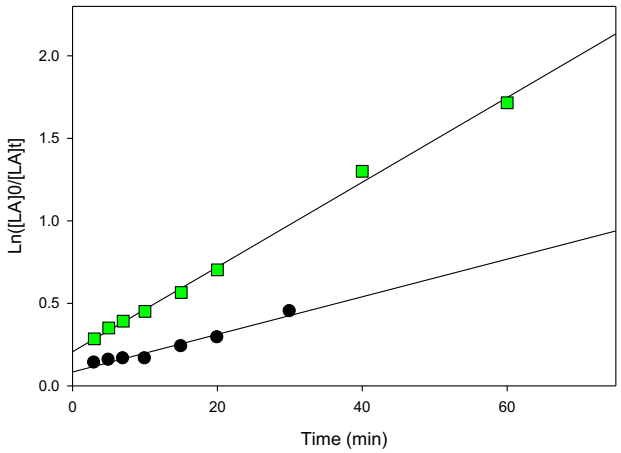

Figure S11. First-order plot of LA consumption initiated by **1**, **2**, **3** and **4** in CH_2Cl_2 under the conditions in Table 2, entries 2, and 13. **1** ($y = 0.0114x + 0.0834$, $R^2 = 0.96$), **3** ($y = 0.0257x + 0.2068$, $R^2 = 0.9983$).

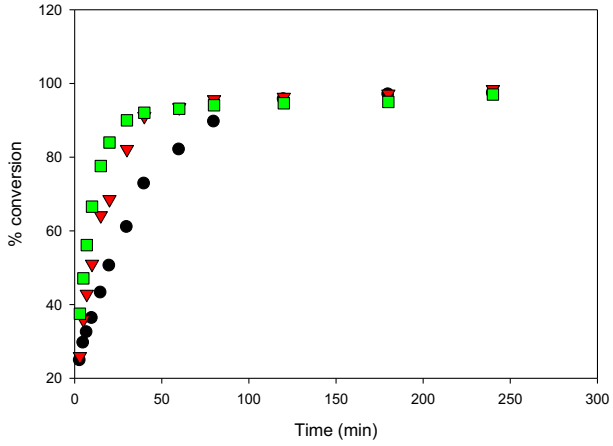

Figure S12. Conversion (%) vs. time for the ROP of LA initiated by **1** in CH_2Cl_2 under the conditions in Table 2, entries 2, 3 and 5. **1 eq. BnOH**, **2 eq. BnOH,** **4 eq. BnOH**.

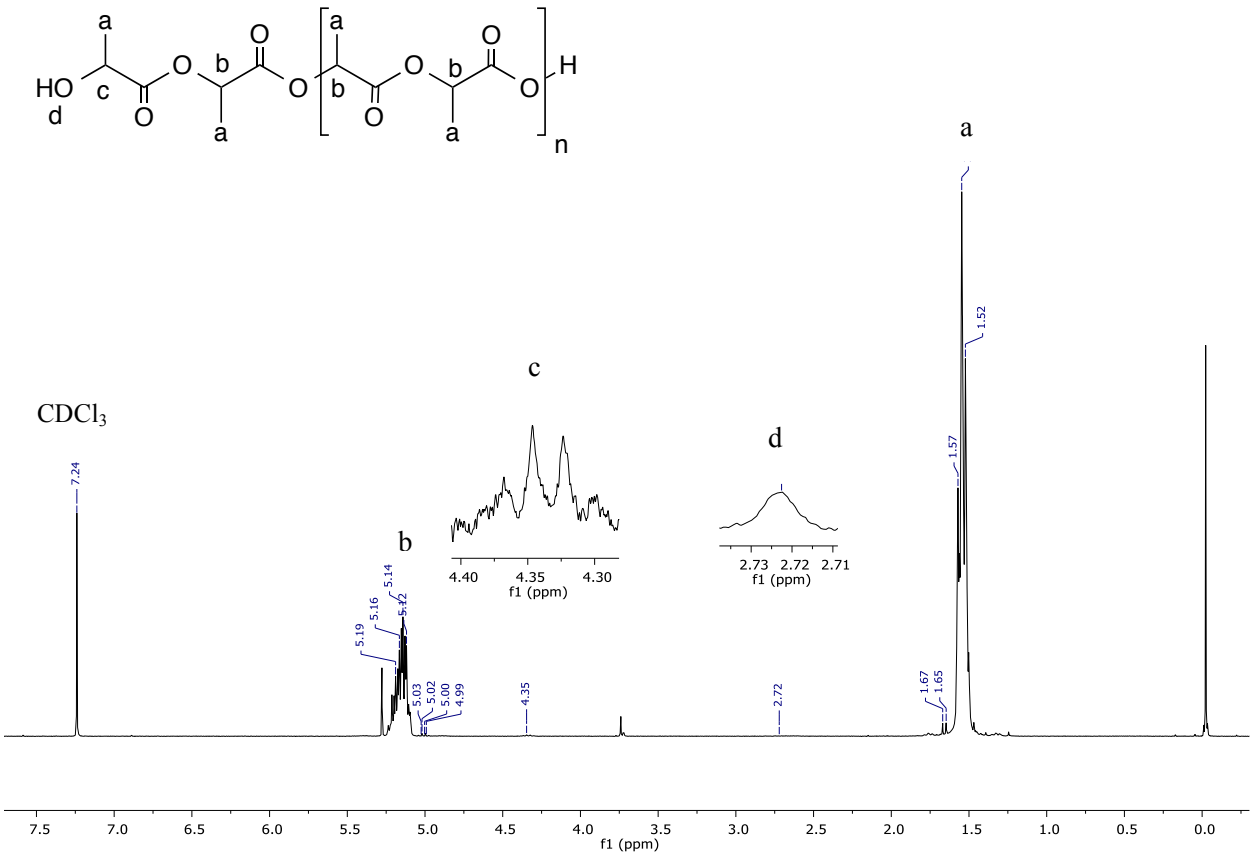

Figure S13. ^{1}H NMR spectrum in $CDCl_3$ of PLA obtained under the conditions in Table 2, entry 12, similar spectra also obtained for entries 13, 18 and 19.

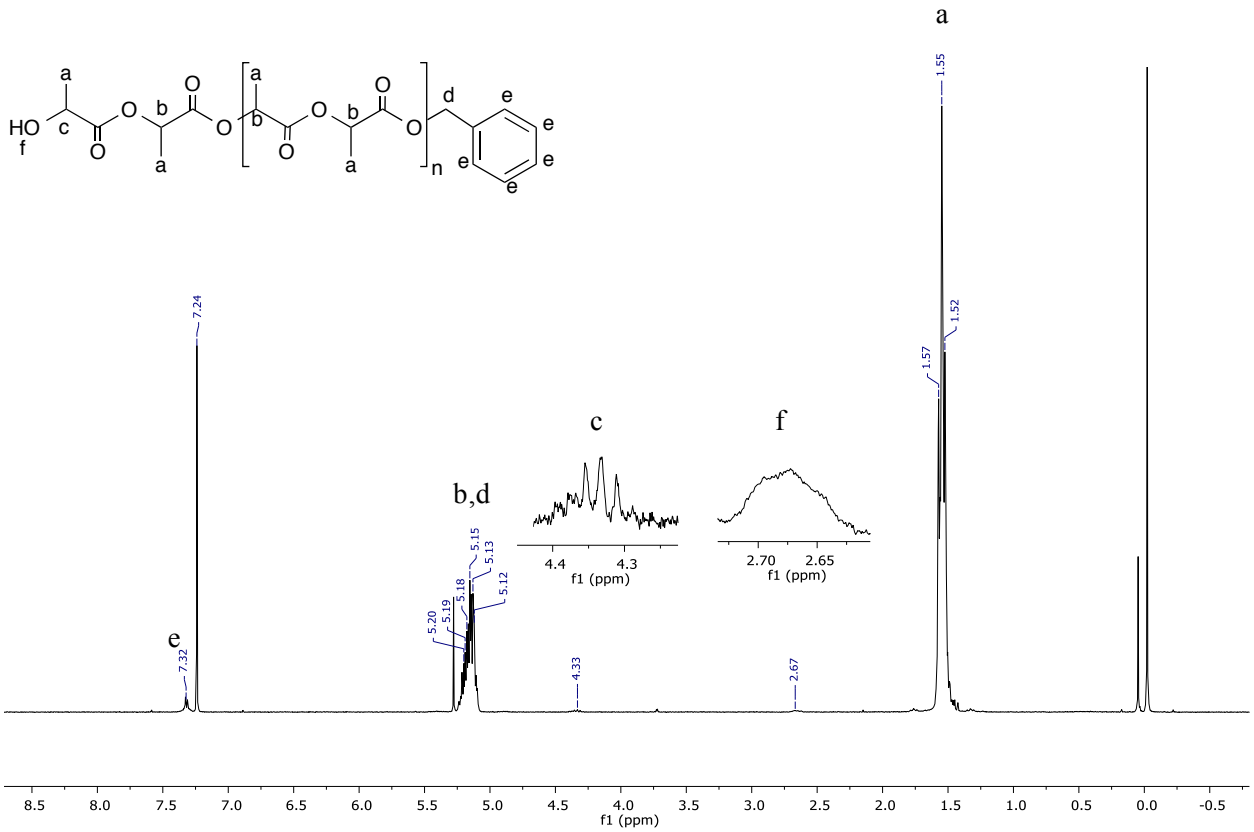

Figure S14. ^{1}H NMR spectrum in $CDCl_3$ of PLA obtained under the conditions in Table 2, entry 3, similar spectrum obtained for entry 5.

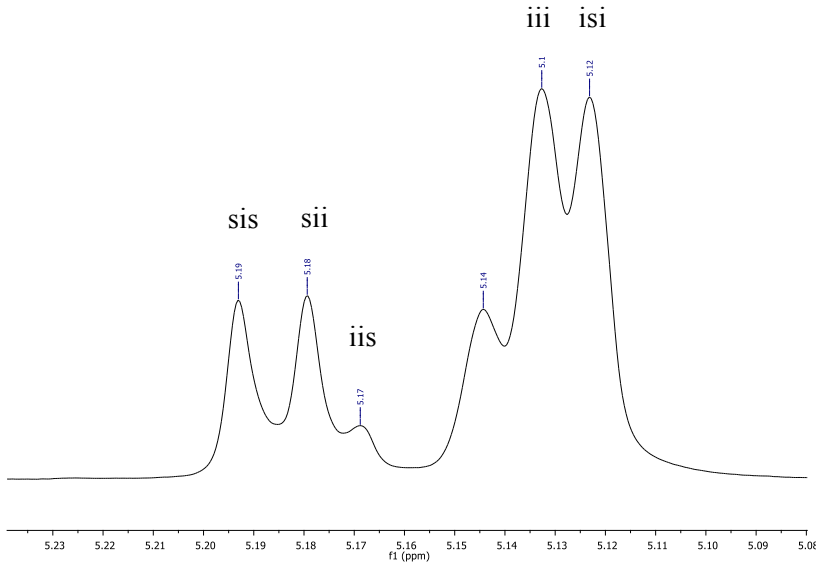

Figure S15. $^{1}H\{^{1}H\}$NMR spectrum (500 MHz, $CDCl_3$) of the methine region of PLA produced under the conditions in Table 2, entry 7, similar results were obtained for entries 8, 12 and 13.

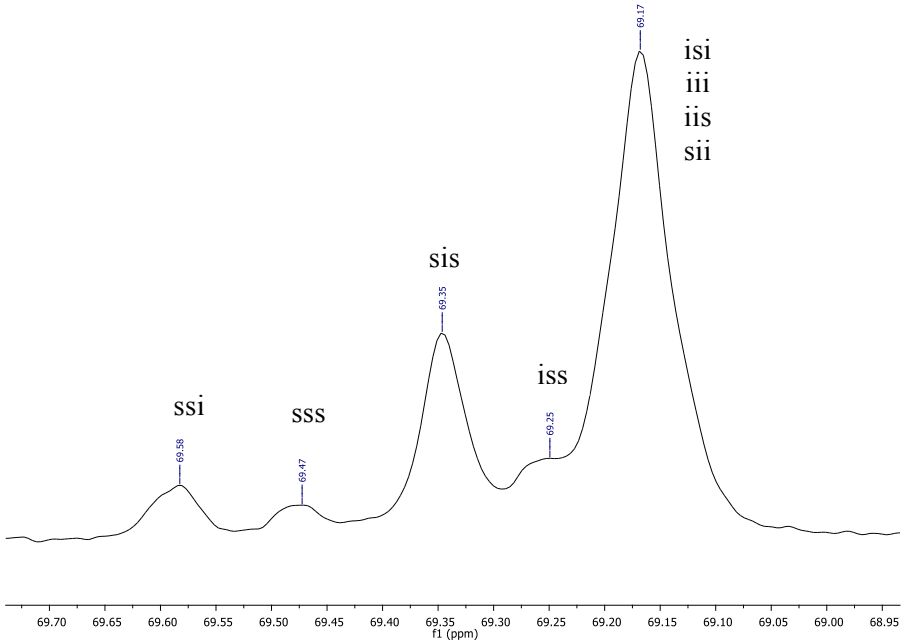

Figure S16. ^{13}C NMR spectrum (500 MHz, $CDCl_3$) of the methine region of PLA produced under the conditions in Table 2, entry 7, similar results were obtained for entries 8, 12 and 13.

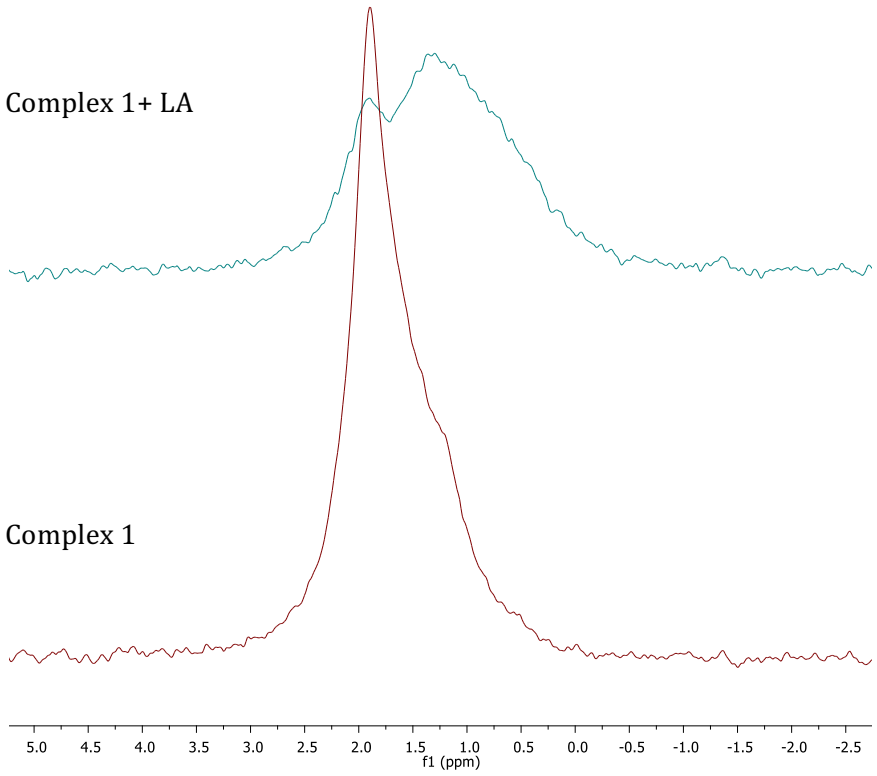

Figure S17. ^{7}Li NMR spectrum (300 MHz, C_6D_6) of **1** with and without 1 equiv. *rac*-lactide.

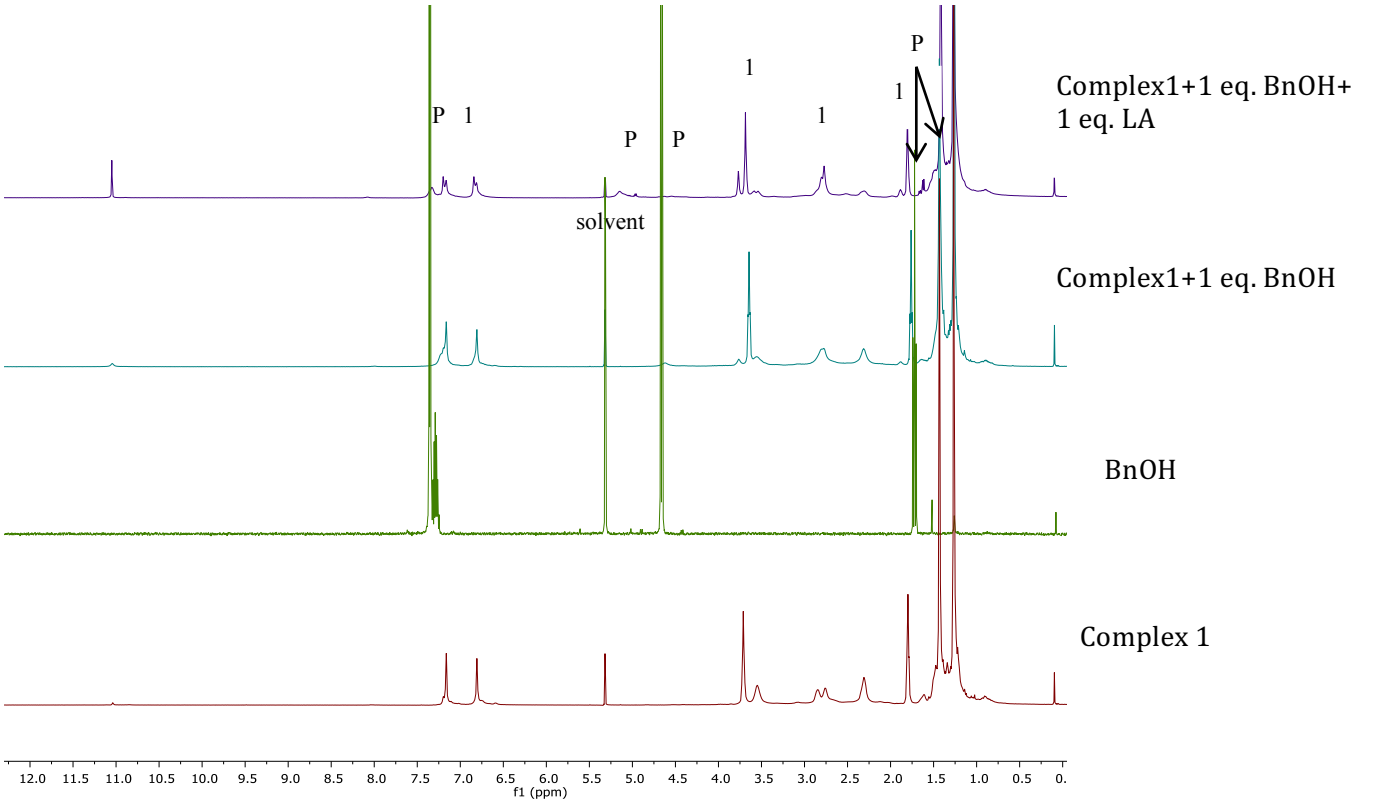

Figure S18. Monitoring of stoichiometric (M: BnOH: LA, 1:1 and 1:1:1) model reactions by ^{1}H NMR in dichloromethane-d_2 at 298 K (500 MHz).

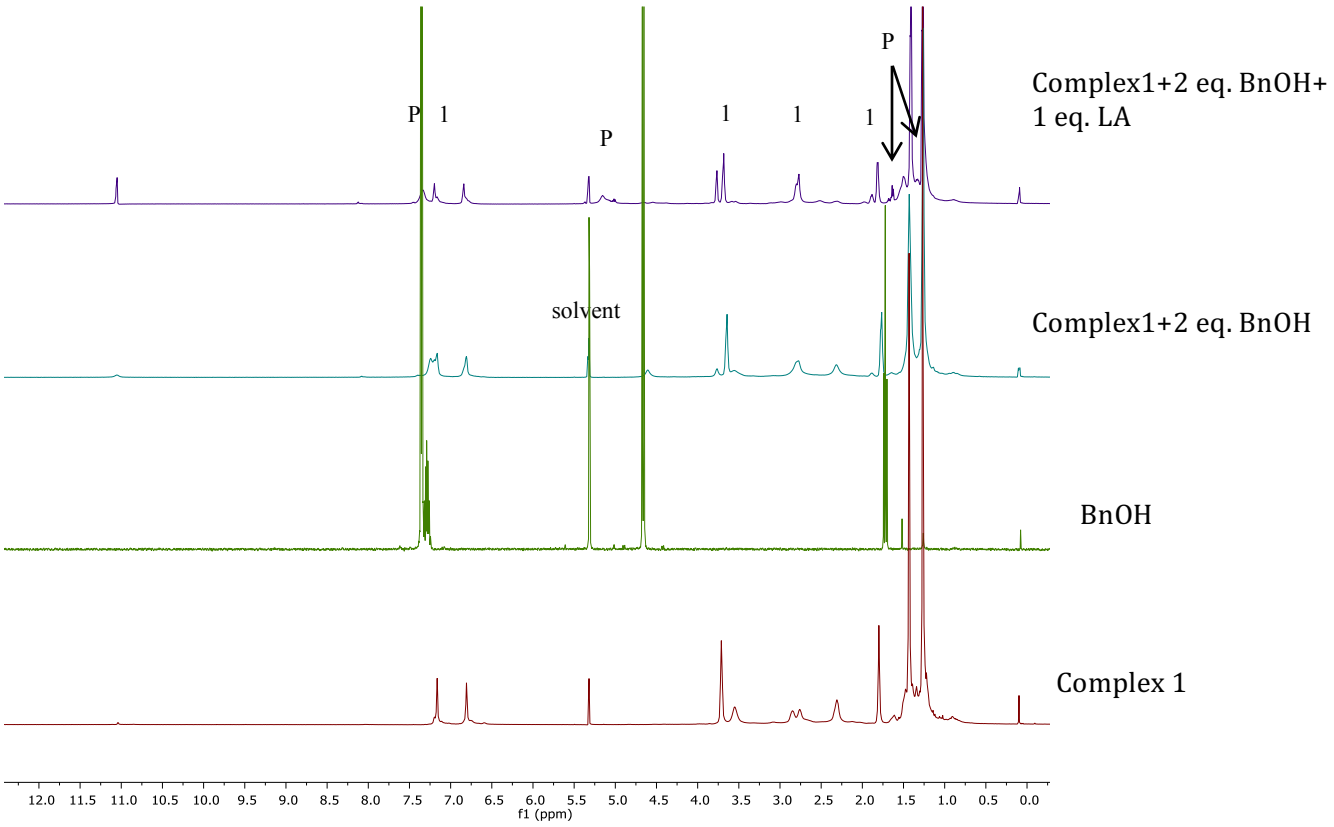

Figure S19. Monitoring of stoichiometric (M: BnOH: LA, 1:2 and 1:2:1) model reactions by ^{1}H NMR in dichloromethane-d_2 at 298 K (500 MHz).

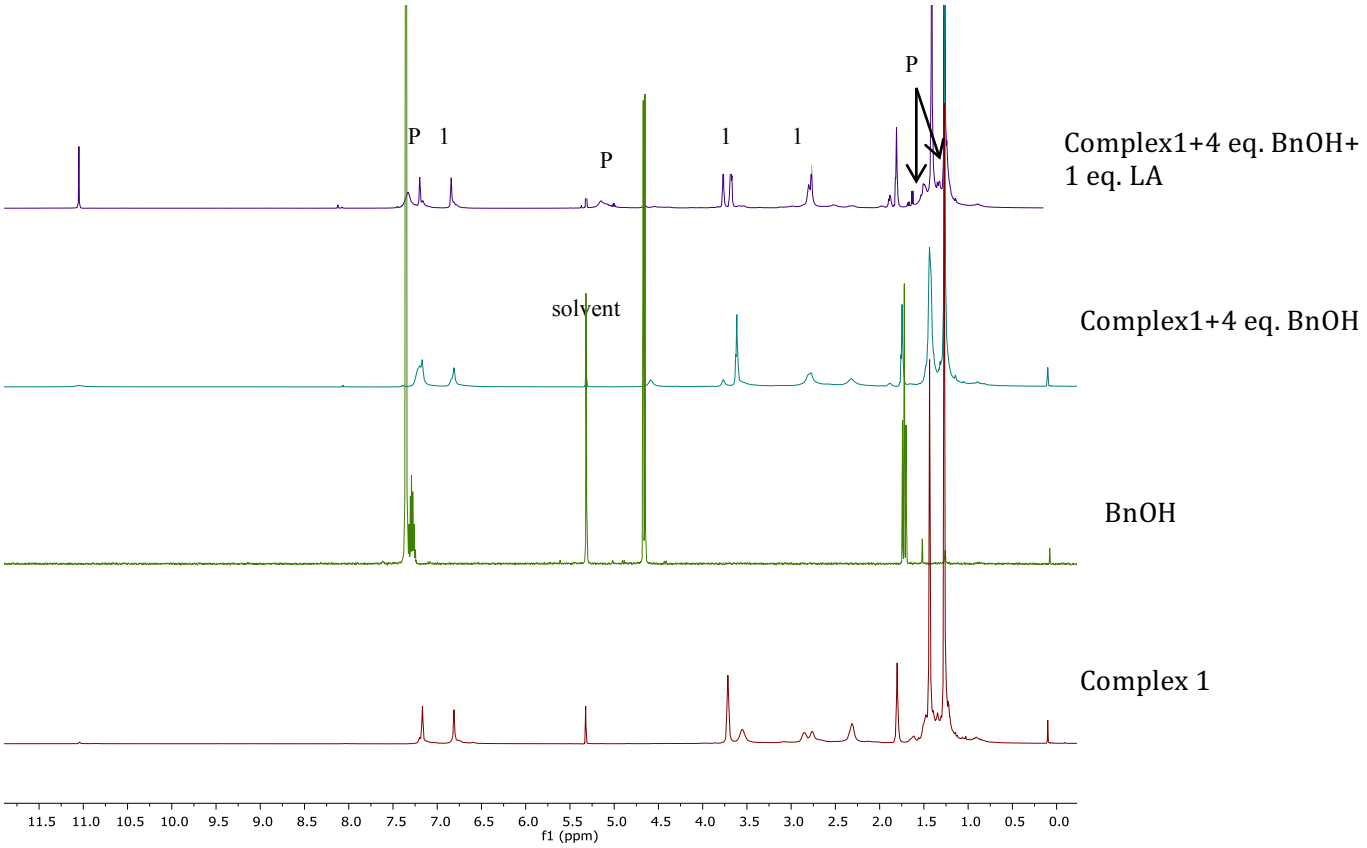

Figure S20. Monitoring of stoichiometric (M: BnOH: LA, 1:4 and 1:4:1) model reactions by ^{1}H NMR in dichloromethane-d_2 at 298 K (500 MHz).

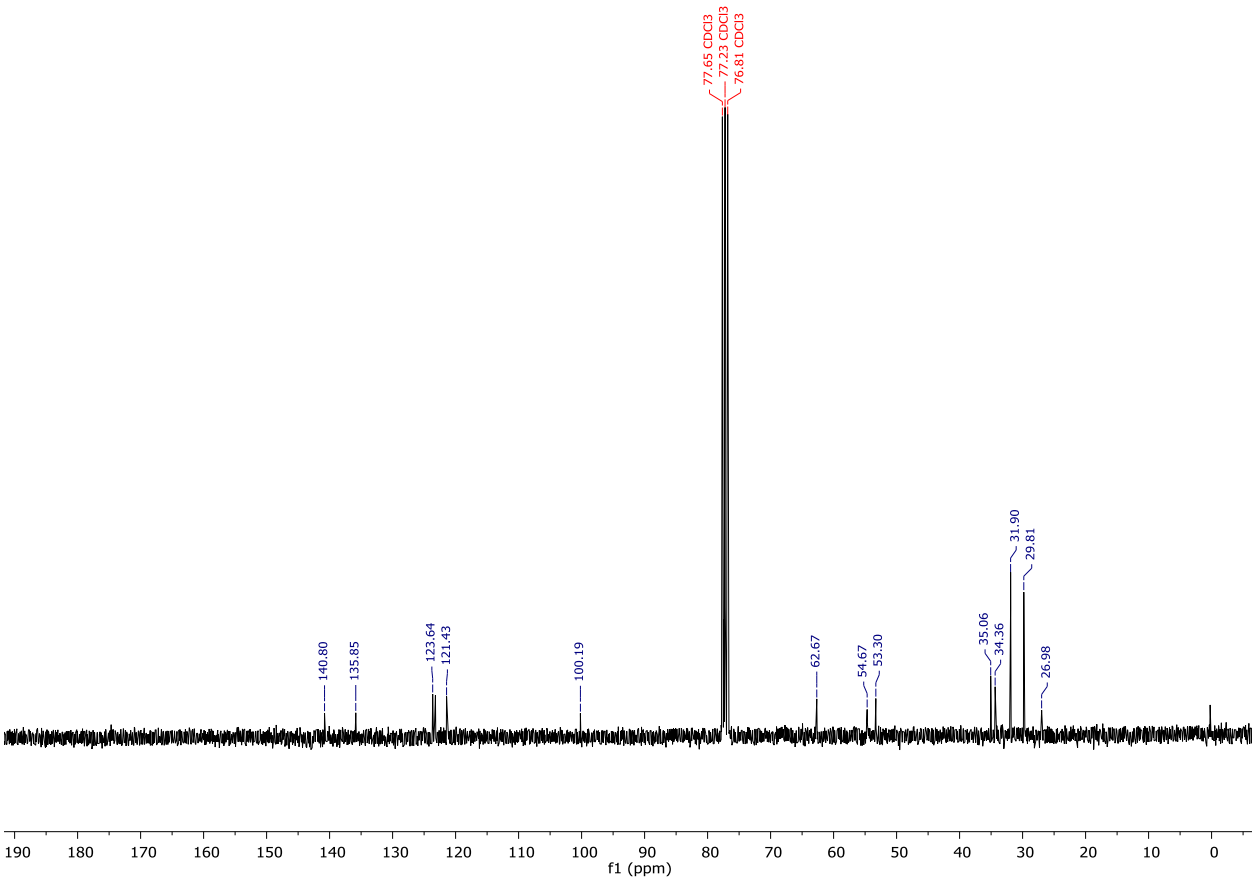

Figure S21. ^{13}C NMR spectrum (300 MHz, 298 K, $CDCl_3$) of **1**.

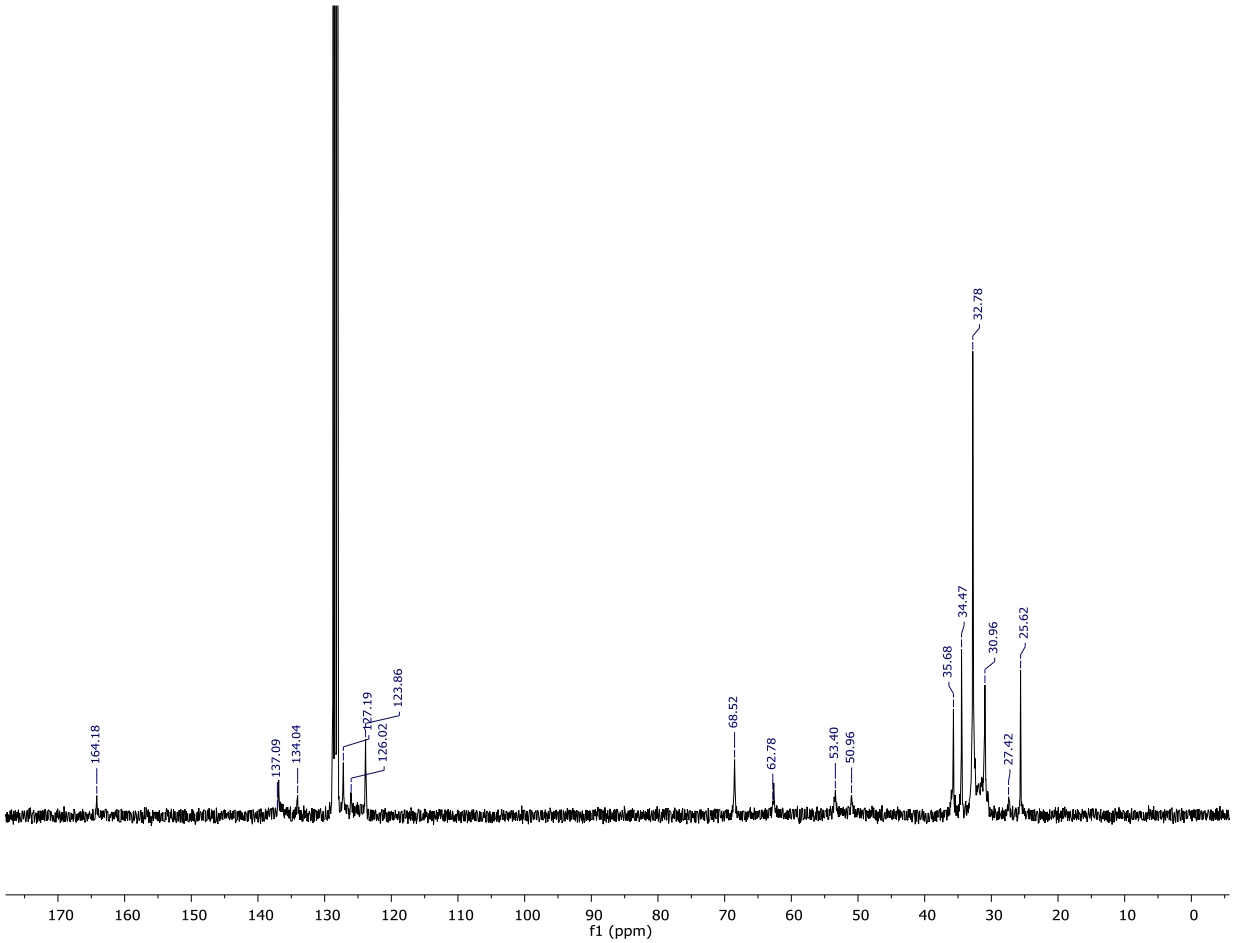

Figure S22. ^{13}C NMR spectrum (300 MHz, 298 K, C_6D_6) of **1**.

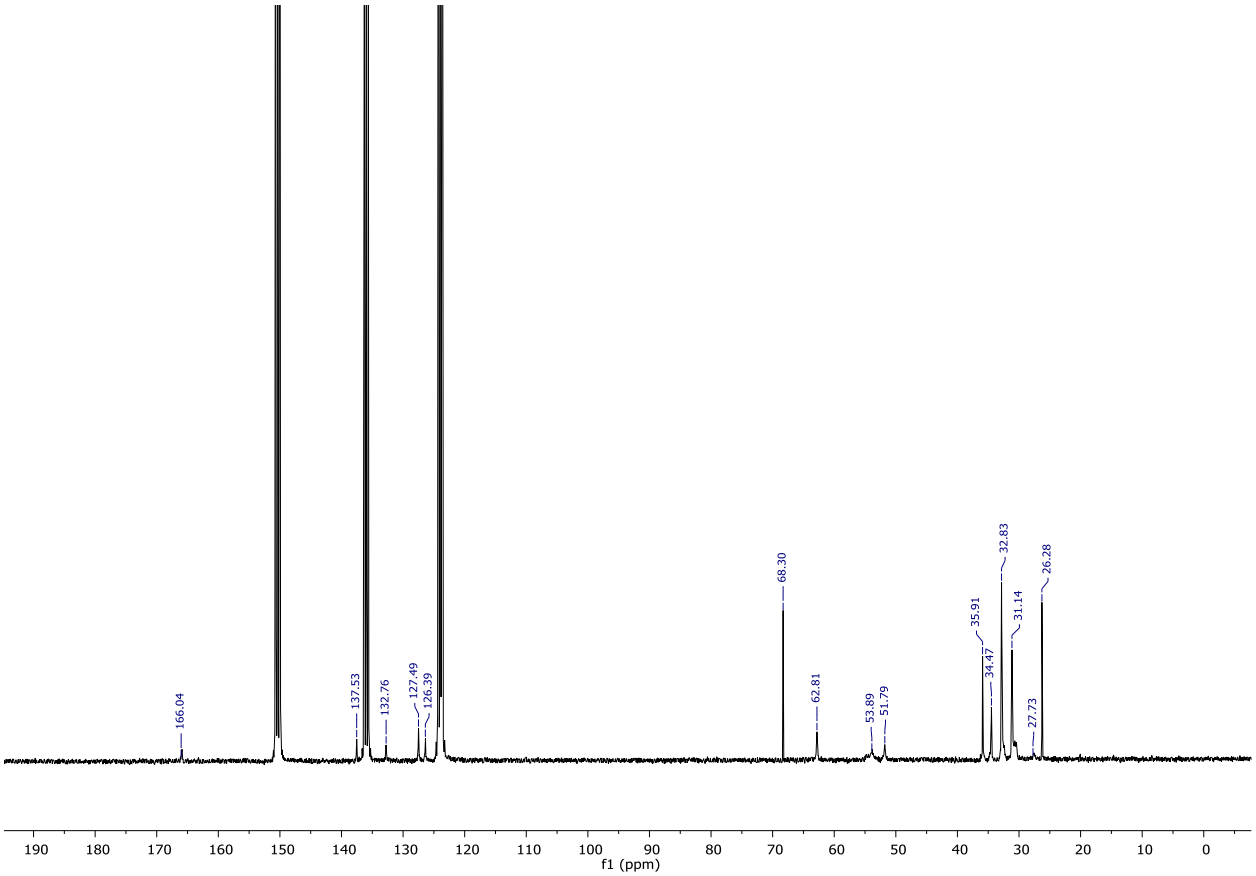

Figure S23. ^{13}C NMR spectrum (300 MHz, 298 K, C_5D_5N) of **1**.

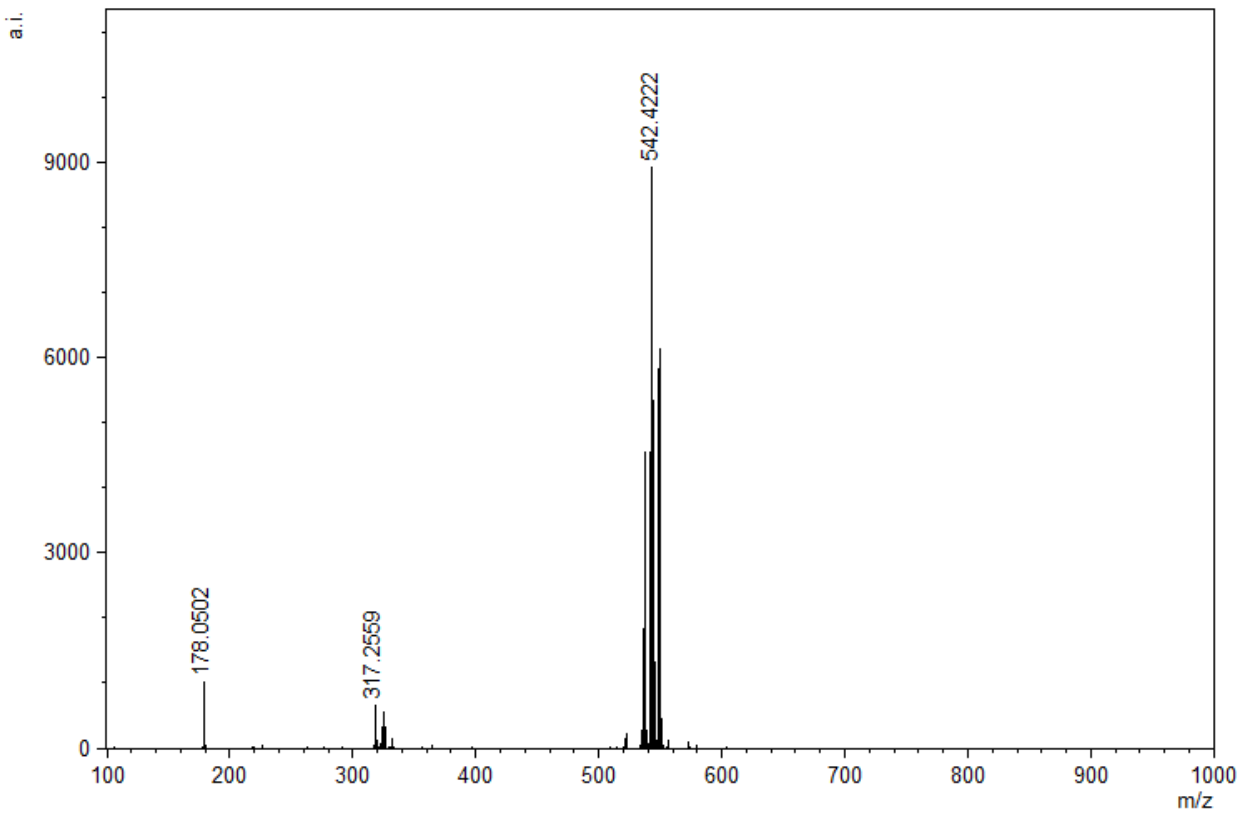

Figure S24. MALDI-TOF spectrum of **1**.

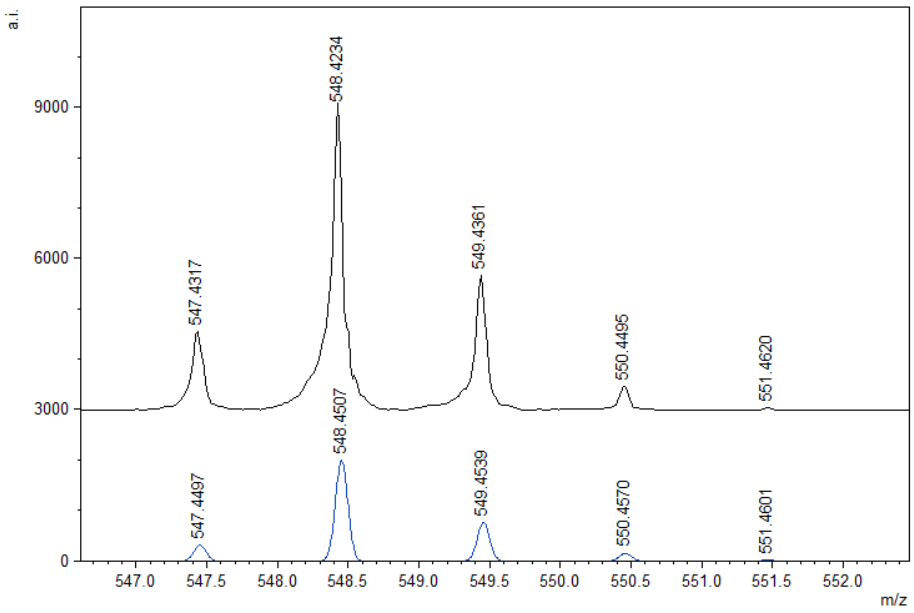

Figure S25. Theoretical and Experimental MALDI-TOF MS isotopic distribution pattern for **1**.

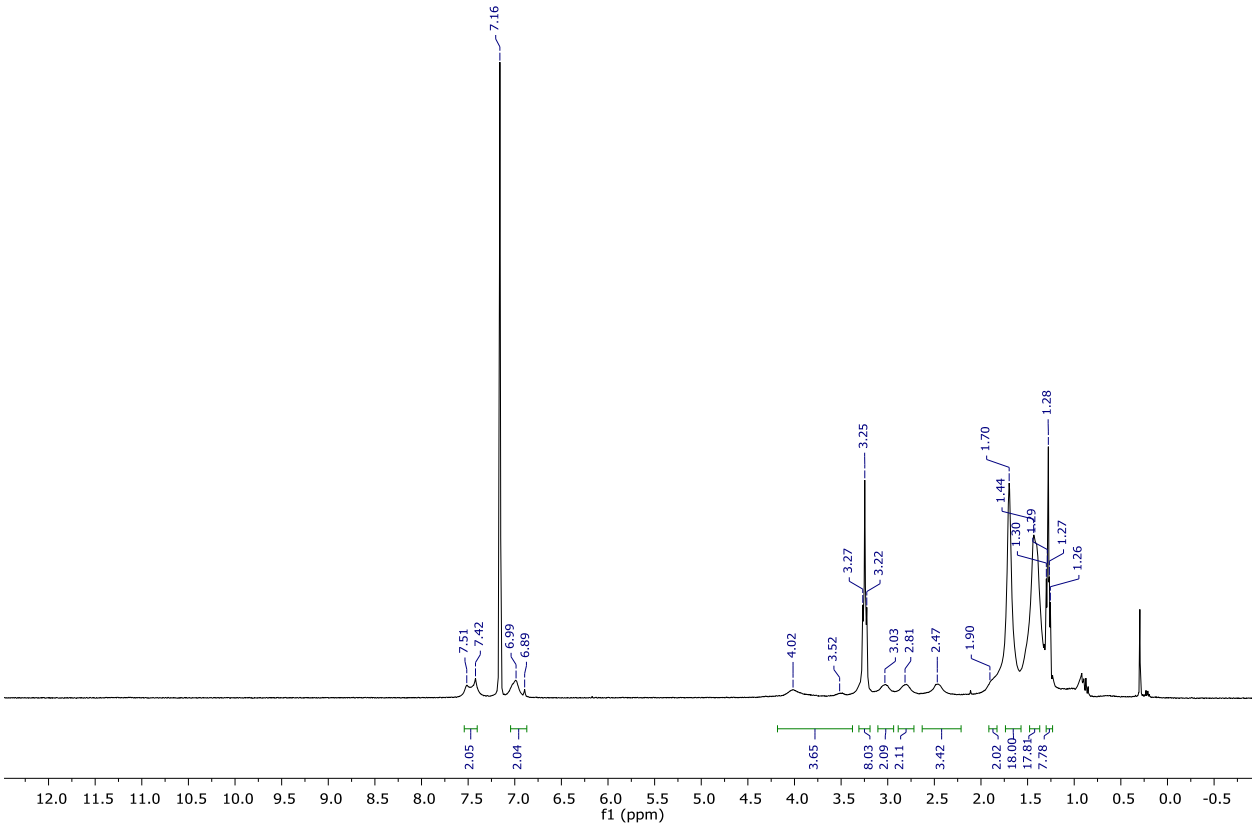

Figure S26. ^{1}H NMR spectrum (300 MHz, 298 K, C_6D_6) of **2.**

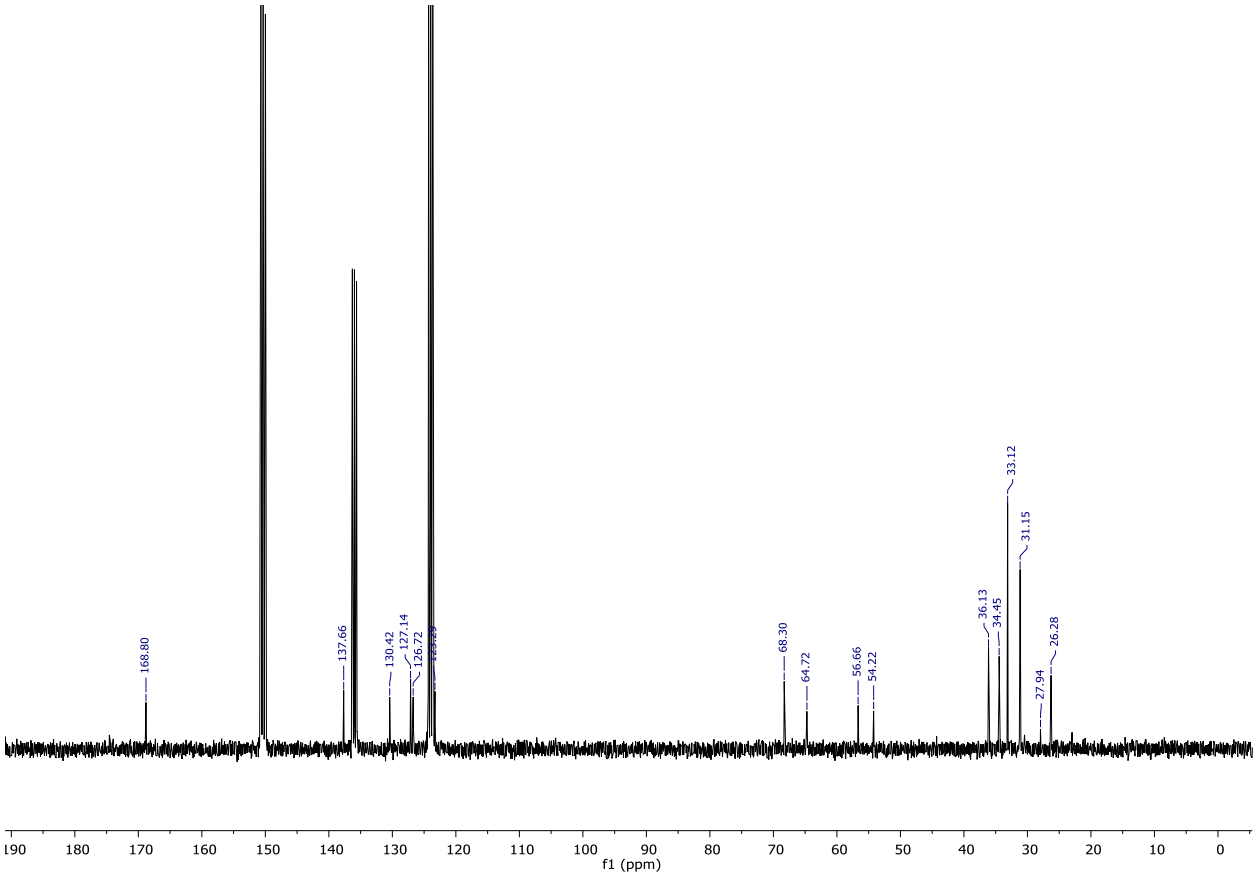

Figure S27. ^{13}C NMR spectrum (300 MHz, 298 K, C_5D_5N) of **2**.

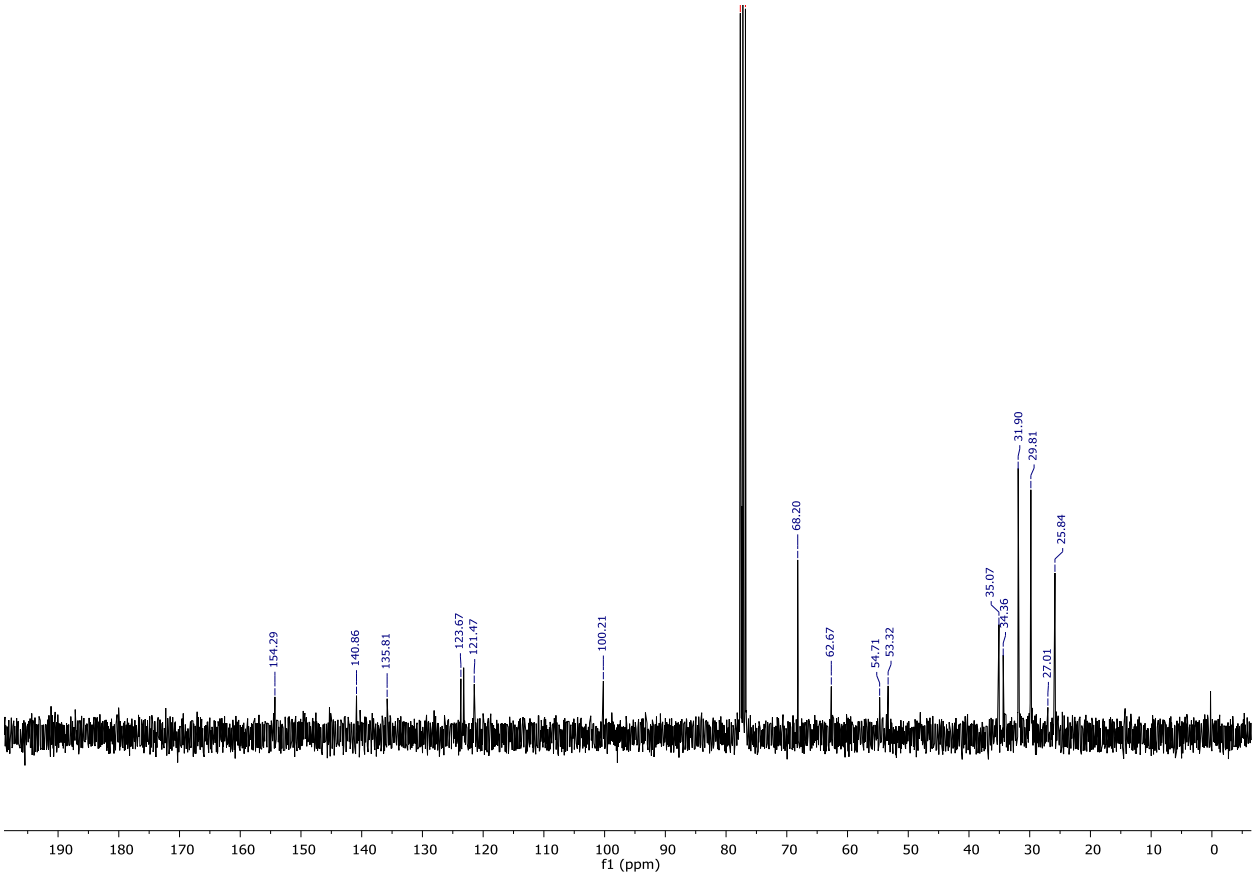

Figure S28. ^{13}C NMR spectrum (300 MHz, 298 K, $CDCl_3$) of **2**.

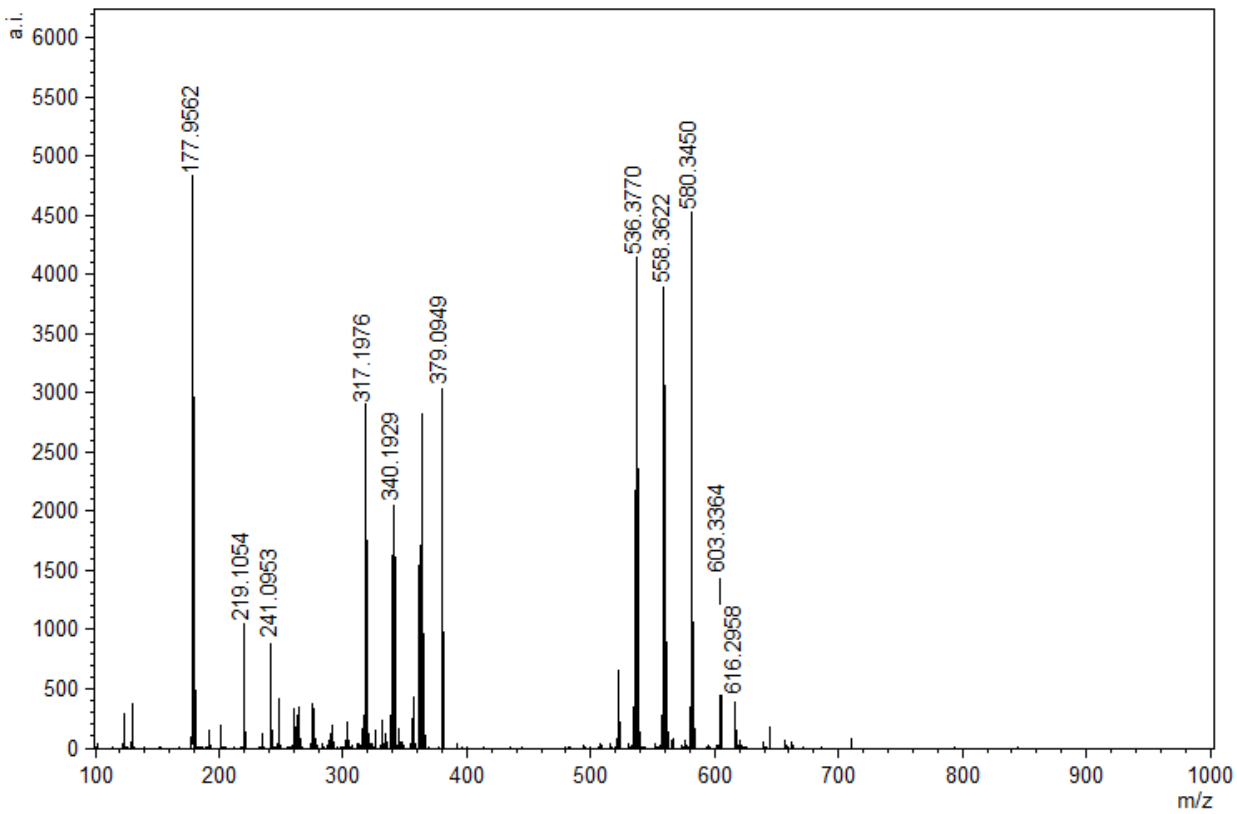

Figure S29. MALDI-TOF spectrum of **2**.

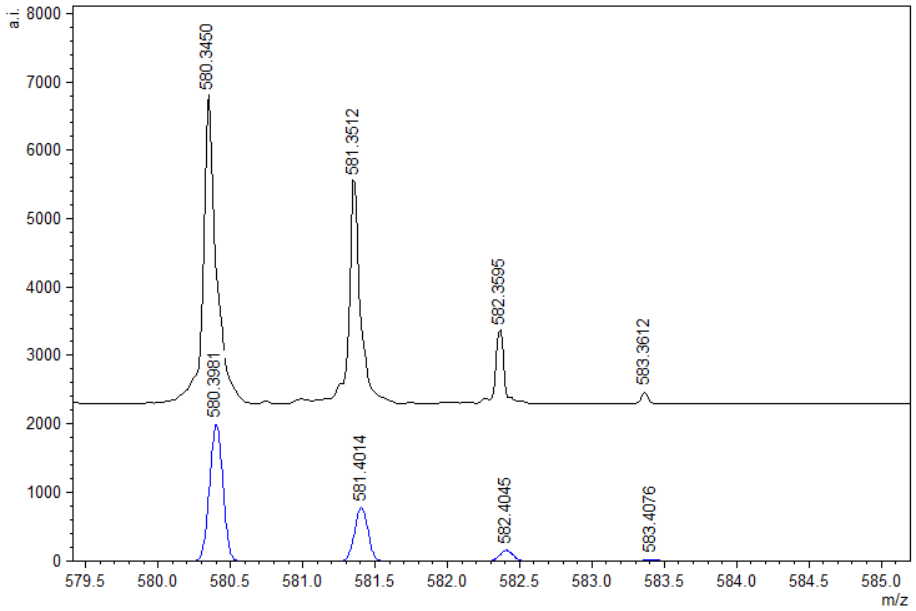

Figure S30. Theoretical and Experimental MALDI-TOF MS isotopic distribution pattern for **2**.

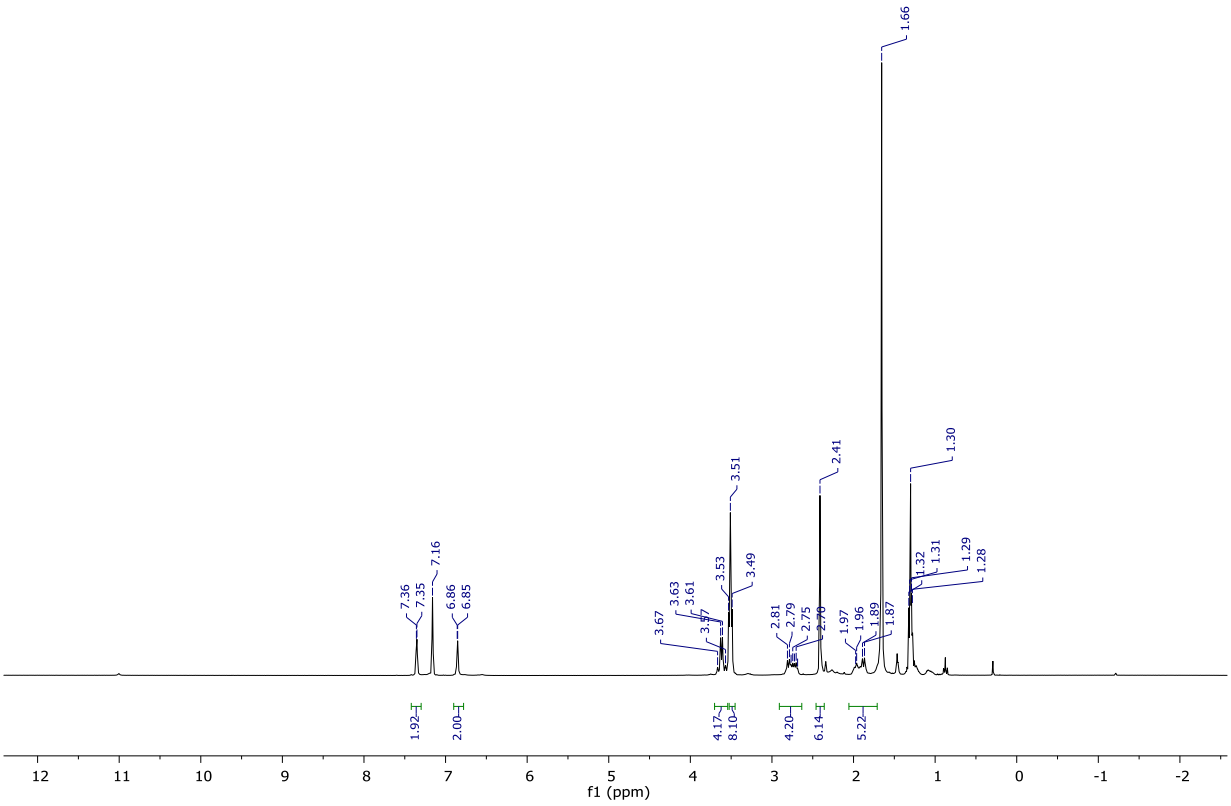

Figure S31. ^{1}H NMR spectrum (300 MHz, 298 K, C_6D_6) of **3**.

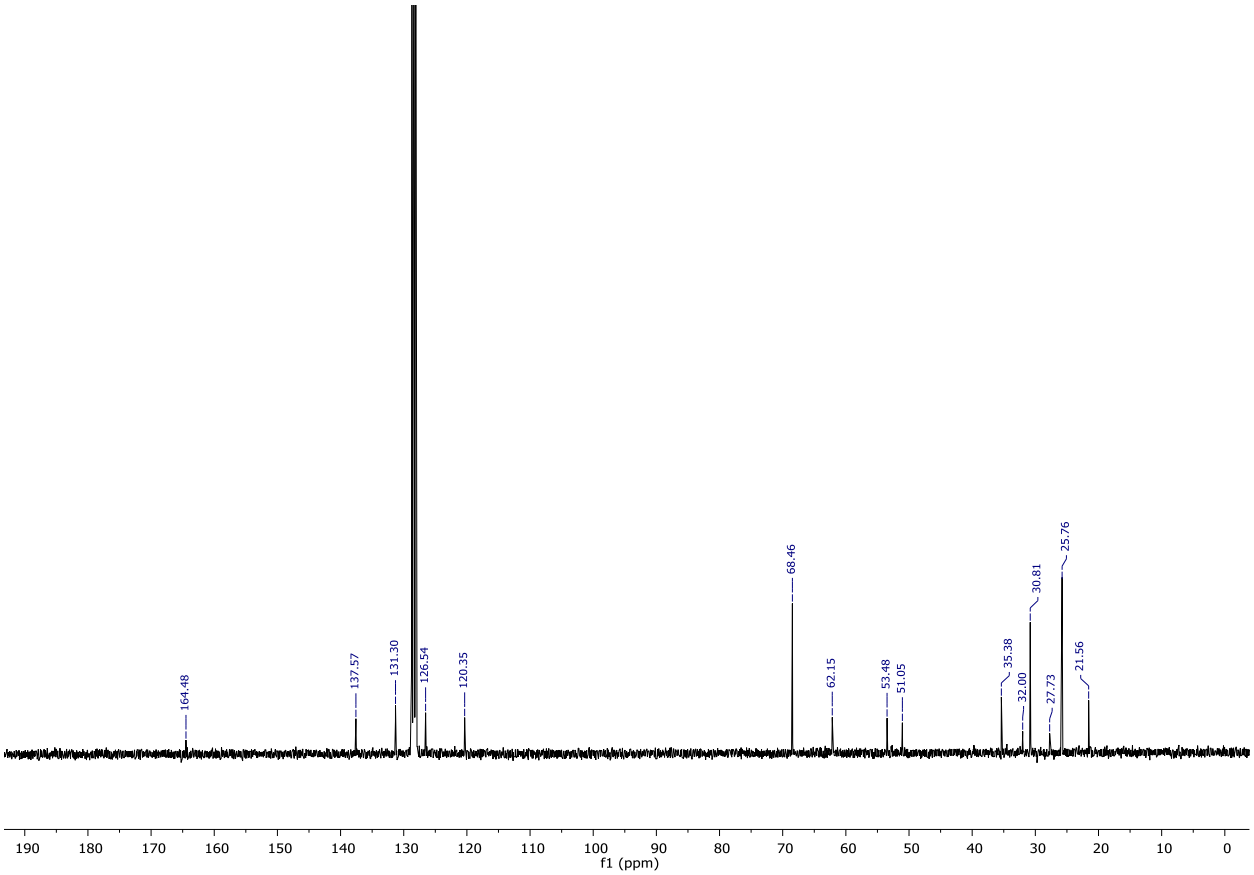

Figure S32. ^{13}C NMR spectrum (300 MHz, 298 K, C_6D_6) of **3**.

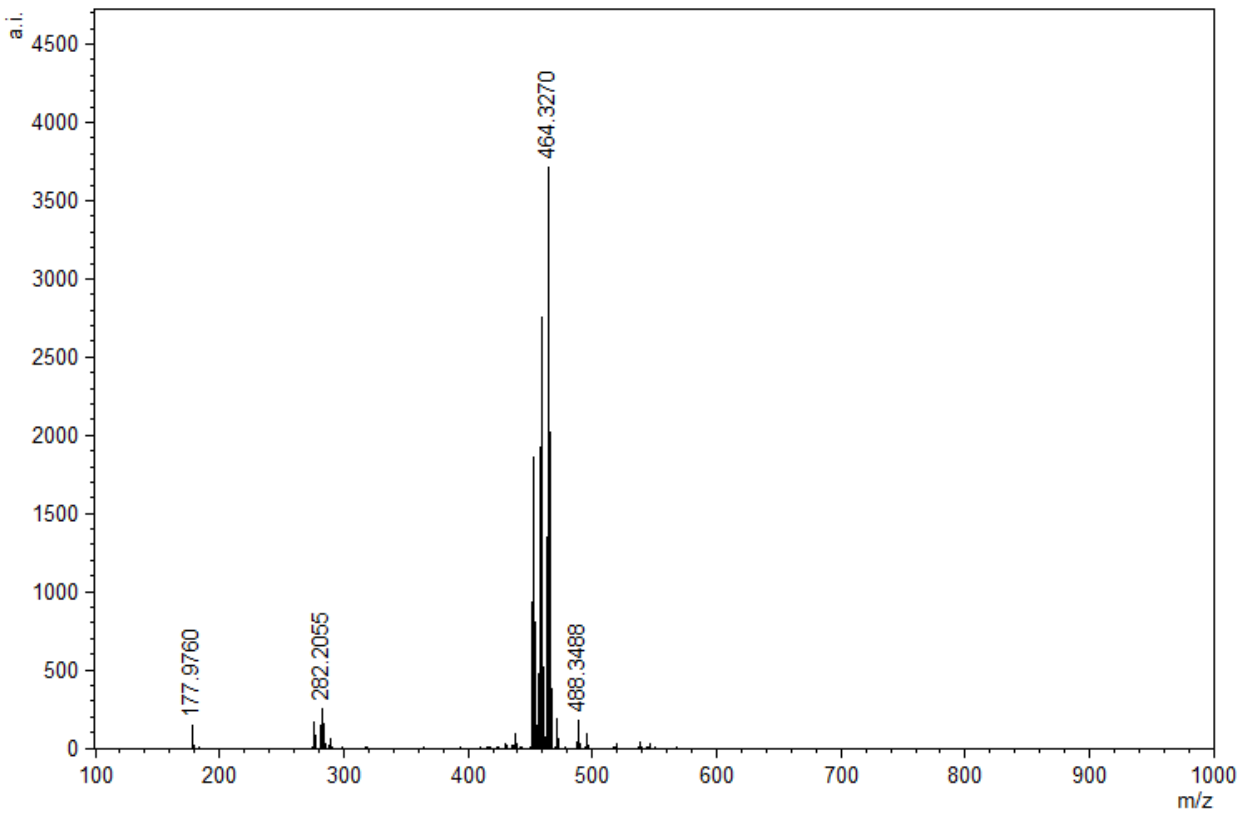

Figure S33. MALDI-TOF spectrum of **3**.

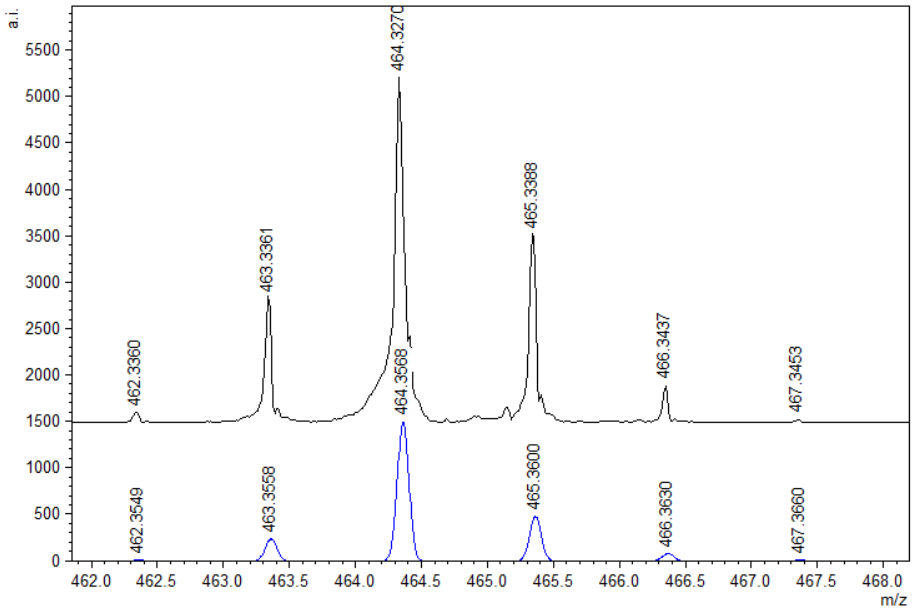

Figure S34. Theoretical and Experimental MALDI-TOF MS isotopic distribution pattern for **3**.

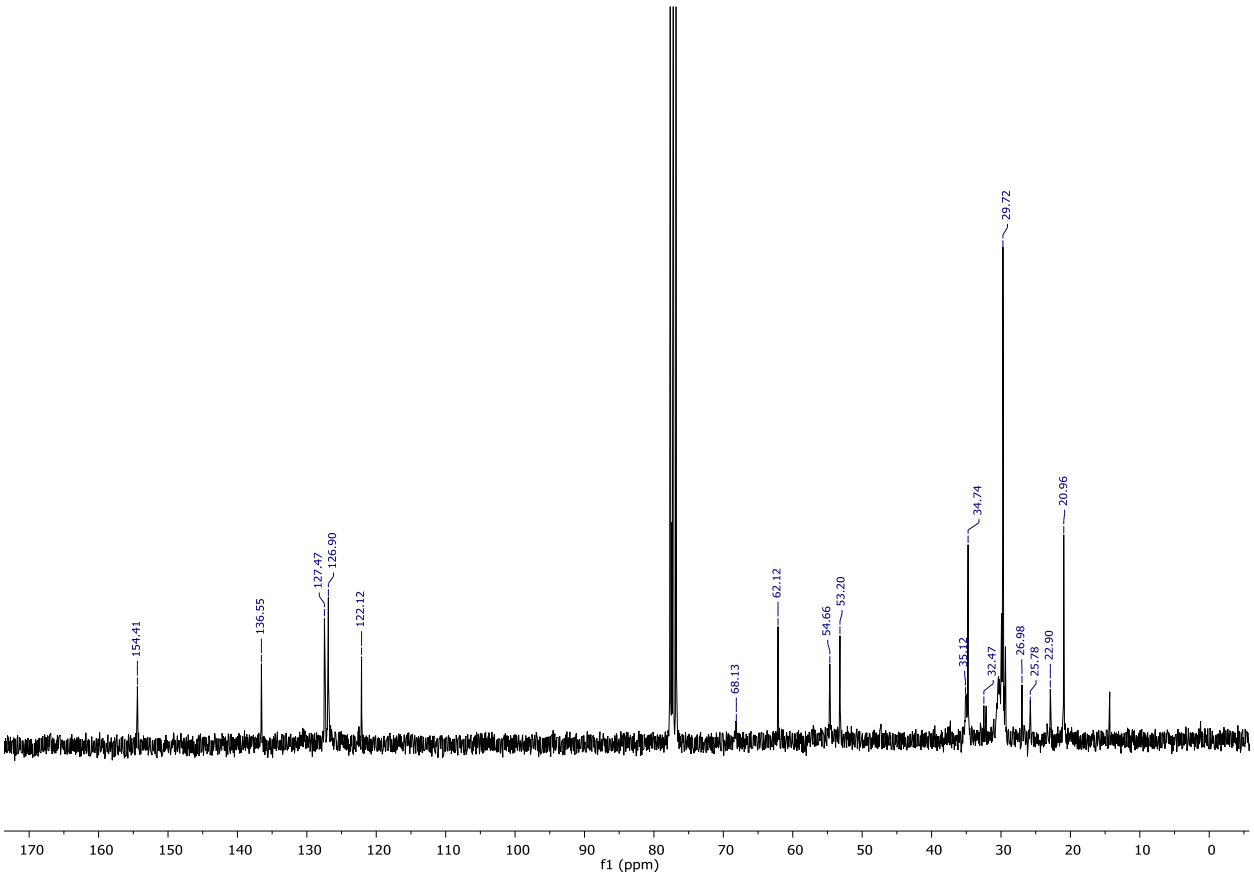

Figure S35. ^{13}C NMR spectrum (300 MHz, 298 K, $CDCl_3$) of 4.

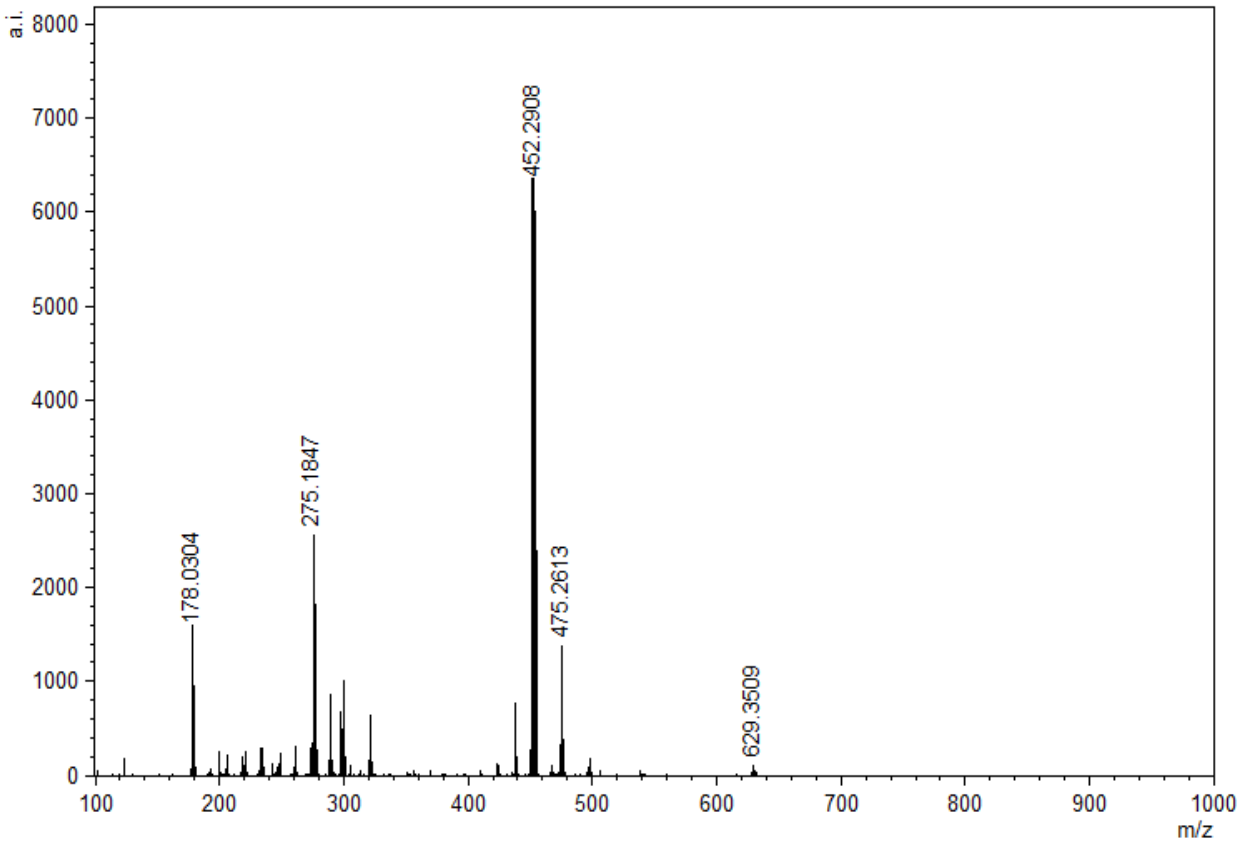

Figure S36. MALDI-TOF spectrum of **4**.